

We are IntechOpen, the world's leading publisher of Open Access books Built by scientists, for scientists

6,000

Open access books available

147,000

International authors and editors

185M

Downloads

Our authors are among the

154

Countries delivered to

TOP 1%

most cited scientists

12.2%

Contributors from top 500 universities



WEB OF SCIENCE™

Selection of our books indexed in the Book Citation Index
in Web of Science™ Core Collection (BKCI)

Interested in publishing with us?
Contact book.department@intechopen.com

Numbers displayed above are based on latest data collected.
For more information visit www.intechopen.com



Chapter

Boron Clusters in Biomedical Applications: A Theoretical Viewpoint

*Ehsan Shakerzadeh, Elham Tahmasebi, Long Van Duong
and Minh Tho Nguyen*

Abstract

In this chapter, we presented an analysis of the recent advances in the applications of boron clusters in biomedical fields such as the development of biosensors and drug delivery systems on the basis of quantum chemical calculations. Biosensors play an essential role in many sectors, e.g., law enforcement agencies for sensing illicit drugs, medical communities for detecting overdosed medications from human and animal bodies, etc. The drug delivery systems have theoretically been proposed for many years and subsequently implemented by experiments to deliver the drug to the targeted sites by reducing the harmful side effects significantly. Boron clusters form a rich and colorful family of atomic clusters due to their unconventional structures and bonding phenomena. Boron clusters and their complexes have various biological activities such as the drug delivery, imaging for diagnosis, treatment of cancer, and probe of protein-biomolecular interactions. For all of these reactivities, the interaction mechanisms and the corresponding energetics between biomaterials and boron clusters are of essential importance as a basic step in the understanding, and thereby design of relevant materials. During the past few years, attempts have been made to probe the nature of these interactions using quantum chemical calculations mainly with density functional theory (DFT) methods. This chapter provides a summary of the theoretical viewpoint on this issue.

Keywords: boron clusters, drug delivery systems, biosensors, quantum chemical computations

1. Introduction

Nowadays, nanomaterials have been applied in most major scientific and industrial fields [1–5]. Such wide ranges of applications are possible owing to the opportuneness of the extremely different classes of nanomaterials with various novel properties. Noticeably, the biocompatibility of the nanomaterials is a great issue for the scientists to use them in the biomedical applications including, among others, biosensors and drug delivery systems.

A biosensor is a device that can produce a measurable signal proportional to the concentration of the biological analyte target [6, 7]. Biosensors are one of the most widely studied topics due to their contributions to development of innovative medicines, which could be applied as adapted drugs or highly sensitive detectors of disease markers [8–15].

Biosensors become new inventions that are hopeful to help an effective diagnosis in the current COVID-19 pandemic and also to remove experimental drugs during the human trials when they show any unwanted adverse effect [16–18]. Generally, a given biosensor has three components including a biological element, a transducer, and a detector [19]. The biological element leads to a detection of the analyte and a generation of a response. This response is thereafter transformed into a detectable signal through a transducer, which is often the most challenging part. Consequently, the generated signal is intensified and processed via an amplifier for exhibiting it by an electronic display device. **Figure 1** schematically illustrates the various steps of the signal processing in a biosensor.

Nanomedicine emerges as a revolutionary medical technology, particularly in the cancer therapy. Recently, much effort has been devoted to the study of nanostructures for applications in nanomedicine domain owing to their particular role in cancer therapies [20–26]. Undoubtedly, the most challenging task in cancer therapy is the finding of a suitable drug delivery system. As the design of efficient and promising drug delivery systems could be developed on the basis of nanostructures, a survey of the relevant prospective drug delivery agents constitutes a primordial subject [27–29].

A key requirement for a drug delivery system is that the delivery of the drug to the targeted sites needs to be associated with a considerable decrease in adverse effects. It is worth mentioning that the experimental research in this field is rather long and expensive, and thereby computational studies can effectively help experimentalists in the design of nanocarriers [30–45]. In this regard, the nature of the interactions between drugs and nanostructures emerges as an essential step. **Figure 2** represents a schematic boron-based drug delivery system.

Boron is an effective element in a wide range of fields. The history of boron chemistry started from the isolation of a series of simple boranes by Stock and his co-workers [46]. In the last two decades, several types of low-dimensional boron nanomaterials such as nanoclusters, nanowires, nanotubes, nanobelts, nanoribbons, nanosheets, and monolayer crystalline sheets have been experimentally synthesized and characterized [47–57]. These boron-based nanomaterials exhibit different bonding patterns from those of bulk boron crystals that exist as the α -, β -, γ -rhombohedral, and α -tetragonal forms. Accordingly, their resulting unique physical and chemical properties are fascinating from a standpoint of materials science. Noticeably, boron-based nanomaterials, such as clusters, can be used as superatoms or building blocks of other nanostructures with novel functionalities and properties.

Of the various types of boron-based nanomaterials, the pure boron clusters (BC) represent a distinctive category of structures owing to their unconventional structures and bonding patterns. During the past decades, boron-based compounds at the



Figure 1.
Steps of signal processing in a biosensor.

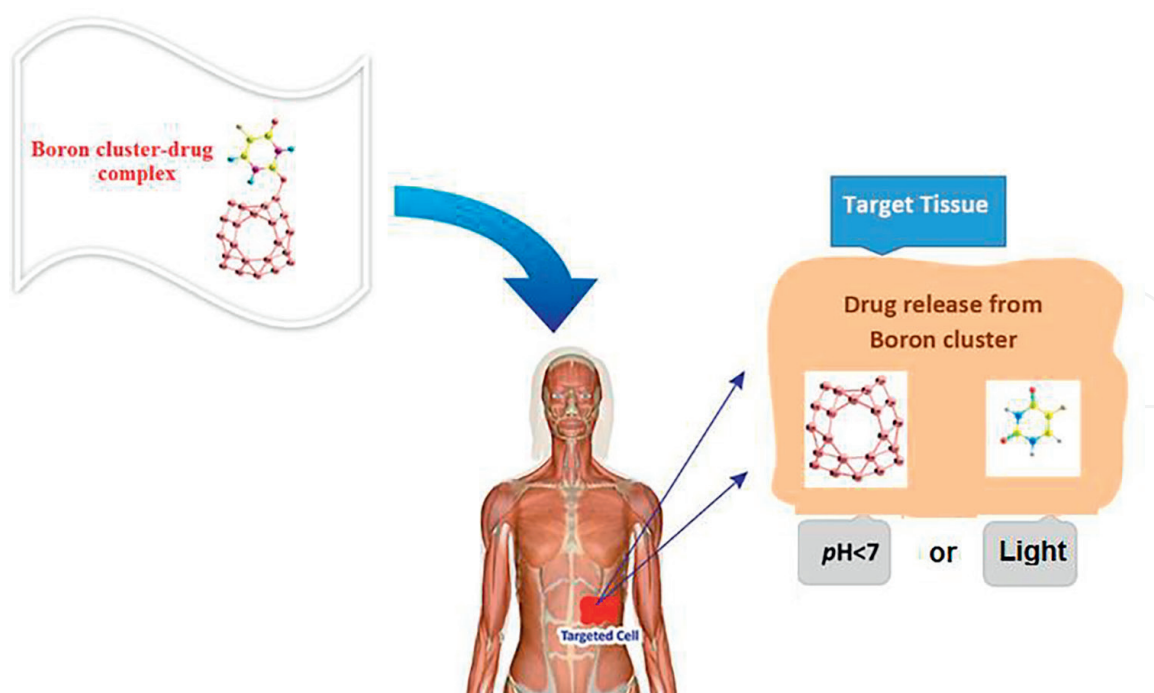


Figure 2.
A schematic boron-based drug delivery system.

nanoscale have been the subject of a large number of theoretical and experimental studies. These systems have intriguing features with different structures such as planar, quasi-planar, ribbon, bowl, cage, teetotum, tubular drum-like forms, multiple ring tubes, and fullerenes [58–72]. This arises from the fact that the boron atom with electron deficiency can take part in both localized and delocalized electronic systems in many geometric shapes. In other words, the most attractive nature of boron skeletons is due to the electron deficiency of the boron atom, leading to a rich bonding capacity.

The neutral B_n clusters with the size of smaller than 20 atoms prefer a planar or quasi-planar structure, except for B_{14} which has a fullerene-type [73]. The B_{40} , $B_{32}C_4$, and $B_{32}Si_4$ fullerene-like clusters together with the B_{30} and B_{36} bowls have attracted some interest in biomedical applications. The schematic structures of B_{40} , $B_{32}C_4$, $B_{32}Si_4$, and B_{36} are provided in **Figure 3**.

Tai et al. [74] reported a computational study on the structural, electronic properties, and chemical bonding of the bowl-like B_{30} global-minimum cluster, exhibiting a disk-aromaticity [11]. Similarly, the B_{36} was theoretically predicted to have a bowl shape stabilized by a disk aromaticity [75]. Piazza et al. [76] subsequently reported an experimental identification of the neutral B_{36} from the photoelectron spectrum of the B_{36}^- anion, confirming a highly stable quasi-planar boron cluster with a central hexagonal hole, providing the first experimental evidence that single-atom layer boron sheets with hexagonal vacancies are potentially viable. The neutral B_{36} is in fact the smallest boron cluster exhibiting a sixfold symmetry and a hexagonal hole, and it can be viewed as a potential basis for extended two-dimensional boron sheets. Recently, it was revealed that the B_{36}^{4-} cluster has a six-membered hole, but the presence of four extra electrons renders the considered system difficult to be synthesized [77]. Thus, the use of carbon or silicon atoms instead of boron anion to neutralize the extra electrons in the carbon or silicon-doped cluster (C_4B_{32} and Si_4B_{32}) has been suggested and comprehensively studied [78].

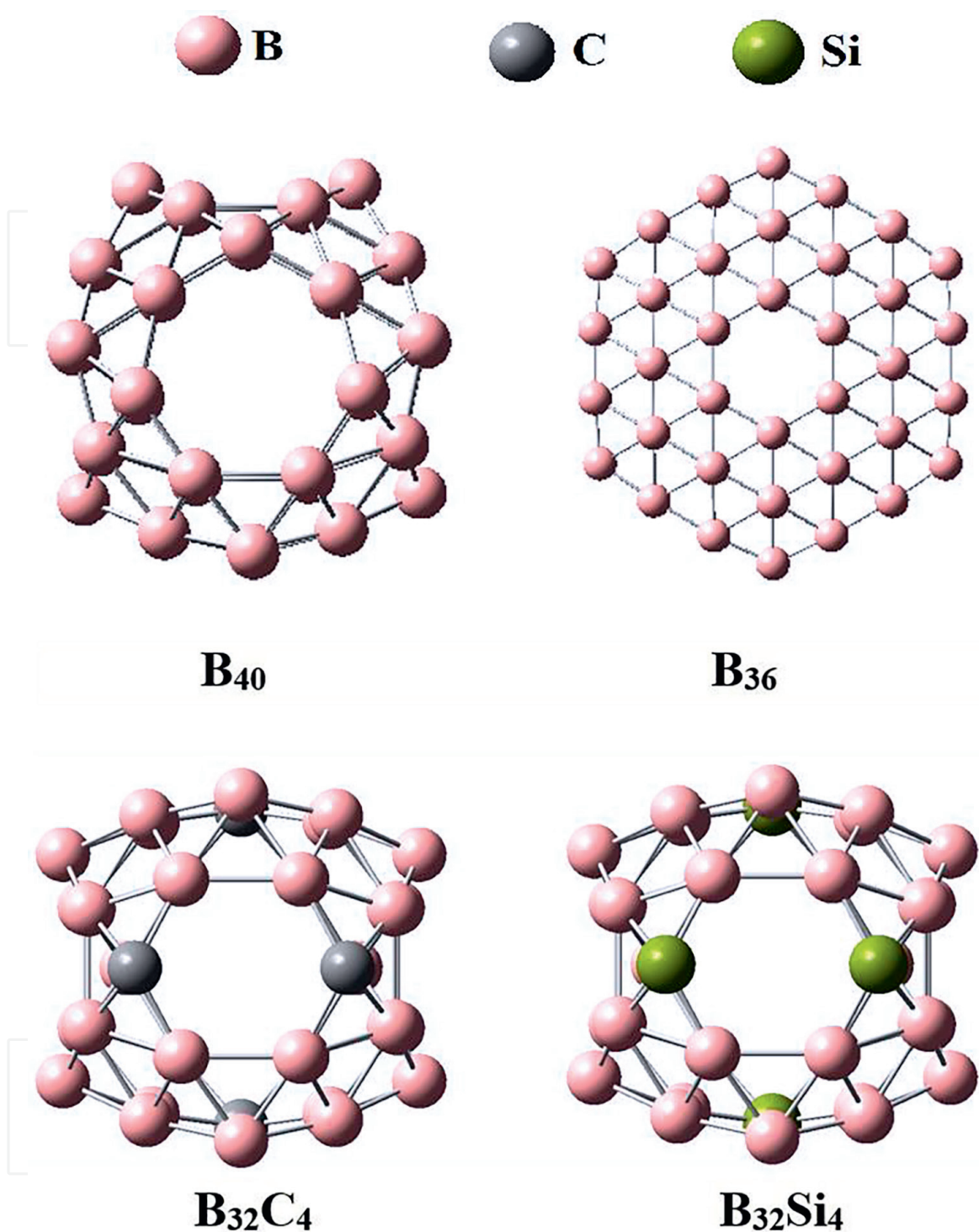


Figure 3.
Shapes of the B_{40} , $B_{32}C_4$, $B_{32}Si_4$ fullerenes, and B_{36} bowl clusters.

The fullerene B_{40} was also predicted by computations [75] and subsequently prepared [79] by utilizing a laser vaporization supersonic source and identified via photoelectron spectroscopy (PES). The B_{40} fullerene with a D_{2d} symmetry consists of four heptagonal rings and two hexagonal rings. With exceptional properties, it has been subjected to many theoretical studies due to its potential applications in molecular devices [80–85]. It is noteworthy that its electronic and reactivity features could be tuned via metal encapsulation or substitution.

Boron neutron capture therapy (BNCT) for cancer treatment remains the main biomedical application of boron-based compounds [86, 87]. Boron compounds have thus facilitated the mission of BNCT. Furthermore, novel biological activities of boron cages and their complexes have been reported [88, 89].

The drugs that are commonly explored for anticancer treatment include 5-fluorouracil (FU), metronidazole (ML), hydroxyurea (HU), nitrosourea (NU), 6-thioguanine (TG), melphalan (MP), and cisplatin and nedaplatin (cf. **Figure 4**). Some nitrosoureas have been used in chemotherapy for treatment of brain tumors, breast carcinoma, lymphomas, and leukemia. The MP drug is conventionally applied for the treatment of specific cancers such as multiple myeloma, ovarian cancer, and breast cancer. FU also has multiple applications and is one of the most beneficial drugs to date to treat breast, head, neck, anal, stomach, colon, and skin cancers [24]. Cisplatin, which is one of the most common anticancer chemotherapy drugs, is particularly effective in treatment of testis, ovary, esophageal, bladder, non-small-cell lung cancers, and head and neck malignancies [90, 91]. Nedaplatin is also an antineoplastic drug which is used for cancer chemotherapy with the

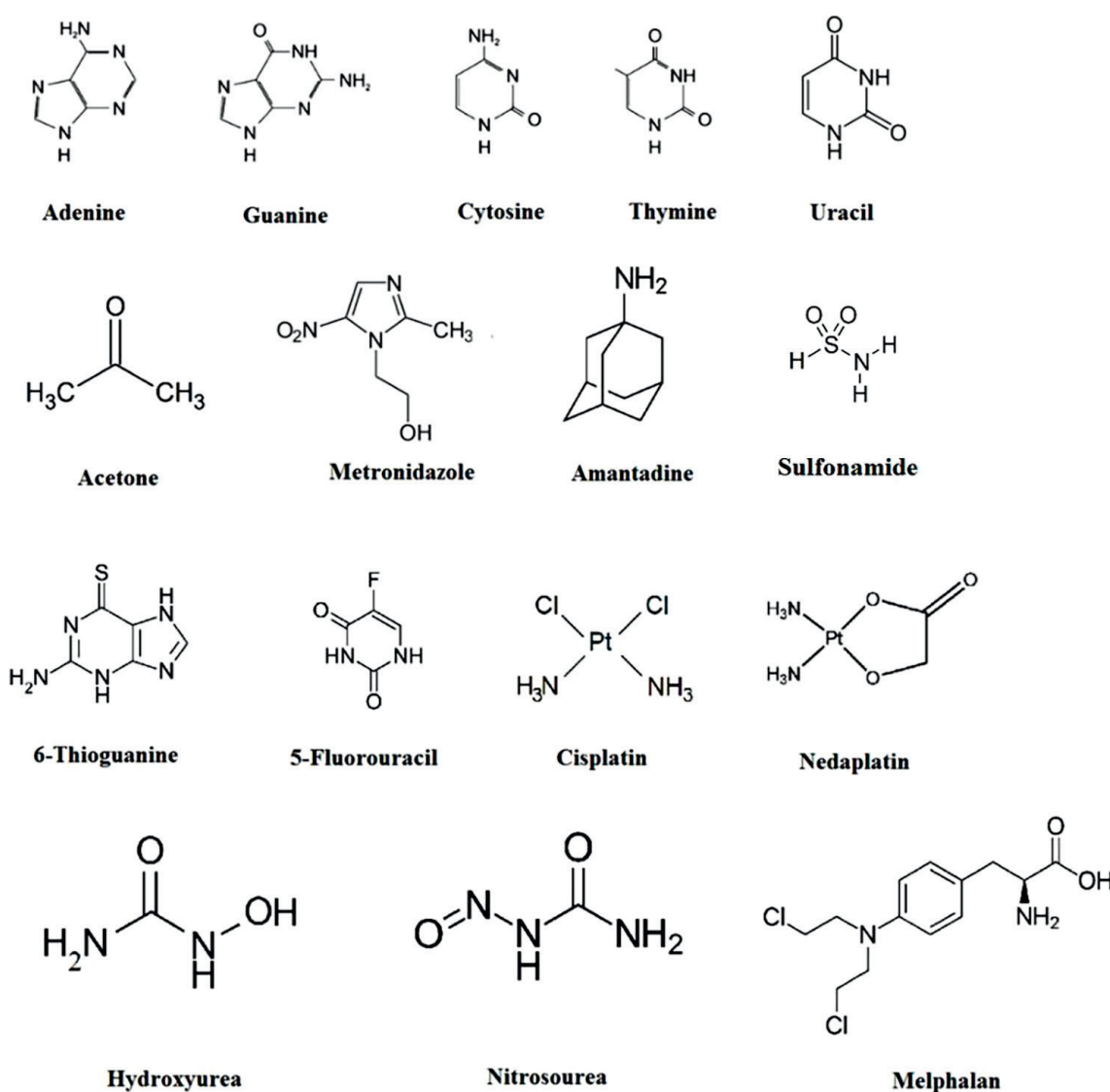


Figure 4. Structures of the biomolecules and drugs commonly considered.

purpose to decrease the inherent toxicities induced by cisplatin [92]. However, the long-term use of such drugs may lead to some secondary tumors such as leukemia [93]. Hence, improvement of the efficacy and reduction of the toxicity of these drugs is of great importance. Of the diverse strategies recently put forward, the drug delivery is one of the most widely used techniques to improve the therapeutic efficiency and targeting of various drugs. In this context, the design of boron-based drug delivery systems appears to be an important issue for the beneficial usage of boron clusters.

The main contribution of this chapter is to scrutinize the functionality of calculated predictions for boron clusters to be considered as prospective biosensors or drug delivery systems. The theoretical methodologies will first be presented. A brief discussion on the various features of promising biosensors or drug delivery systems that should further be investigated for biomedical applications.

2. Methodology

In this section, a brief discussion is presented on the various features of the biosensors and drug delivery systems, that can be predicted using quantum chemical methods. Density functional theory (DFT) ranks as the most widely used quantum mechanical method and plays an increasingly larger role in a number of disciplines besides chemistry, such as physics, materials, biology, and pharmacy [94–103]. While DFT computations have long been used to complement experimental investigations, the approach has emerged as an indispensable and powerful tool for predictions of different fields.

A general theoretical approach to this topic boils down to an assessment of the interactions between the materials and the biomolecules or drugs considered. It simply leads to an examination of the structures and properties of the interacting complexes. This requires a determination of all possible configurations of the complexes by carrying out systematic geometry optimizations and making use of appropriate DFT methods. The nature of local energy minima corresponding to various configurations needs to be verified through an analysis of their vibrational frequencies. In order to assess the capability of a boron cluster for detection of a biomolecule or drug delivery system, the structural, energetic, and electronic properties can simply be computed for the relaxed favorable geometries. These properties can provide us with valuable information for biomedical applications. All the mentioned calculations can be performed in both vacuum and aqueous media. It is essential to evaluate these parameters in aqueous medium since these systems are anticipated to act in human body. The polarizable continuum model (PCM) and the conductor-like screening model (COSMO) are common continuum models for the treatment of the solvent effects. The key factors of the properties mentioned above are described as follows.

2.1 Structural parameters

From an optimized geometry, the bond lengths and bond angles between the constituent atoms in the complexes can be determined. These are simple but essential parameters determining the nature of the interaction between the drug molecules and respective adsorbents.

2.2 Energetic properties

The interaction energy (E_{int}) of a biomolecule or drug with a boron cluster is the key parameter that should be determined in order to emphasize the nature of the interaction. The interaction energy is usually computed as in Eq. (1):

$$E_{\text{int}} = E_{\text{BC-adsorbent}} - E_{\text{BC}} - E_{\text{adsorbate}} \quad (1)$$

where $E_{\text{BC-adsorbent}}$ denotes the total energy of the adduct formed upon interaction between the boron cluster with the corresponding drug or biomolecule. The E_{BC} and $E_{\text{adsorbent}}$ terms correspond to the total energies of the isolated boron cluster and the drug or biomolecule, respectively. These energies are usually calculated using DFT methods. The efficiency of DFT methods, namely the functionals, for evaluating interaction energies was documented previously. The reported results show a good performance with the root-mean-square deviation of 0.05 kcal/mol and the mean absolute deviation of 0.07–0.13 kcal/mol against the benchmark energies of N-methylacetamide-water complex obtained at the CCSD (T)/CBS-aTQ complete basis set limit level [104]. N-methylacetamide is the simplest model for the peptide linkage in peptides and proteins.

As for a convention, a negative interaction energy indicates that the obtained complex is thermodynamically stable, while a positive adsorption energy refers to a local minimum where the interaction is prevented by an energy barrier connecting it with the global minimum. The interaction energy can provide us with meaningful insights to distinguish between a chemisorption and a physisorption process.

The recovery time (τ) is one of the important factors for biomedical applications. It can be used for estimation of the drug desorption from the cluster surface or the sensor refreshing, which can be occurred by exposing to light. Based on the conventional transition state theory, the recovery time can be computed using the Arrhenius-type Eq. (2):

$$\tau = \nu_0^{-1} \exp\left(\frac{-E_{\text{int}}}{kT}\right) \quad (2)$$

where ν_0 , T , and k terms stand for the attempt frequency, the temperature of the system, and the Boltzmann constant, respectively. A larger interaction energy inherently leads to a longer recovery time, which is not a good factor for drug release or for a biosensor refreshing. Thus, the adsorption process energy should be neither chemisorption nor physisorption; it should be in a semi-chemisorption to provide an efficient recovery time. Accordingly, an interaction characterized by a *large interaction energy is not always favorable for biomedical applications*.

It is possible to investigate the thermodynamical nature of the interaction, through the change in the Gibbs energy using Eq. (3):

$$\begin{aligned} \Delta G &= G_{\text{BC-adsorbent}} - G_{\text{BC}} - G_{\text{adsorbate}} \\ &= (H_{\text{BC-adsorbent}} - H_{\text{BC}} - H_{\text{adsorbate}}) - T(S_{\text{BC-adsorbent}} - S_{\text{BC}} - S_{\text{adsorbate}}) \end{aligned} \quad (3)$$

where G represents the sum of electronic and thermal free energies. H stands for the sum of electronic and thermal enthalpies. S and T refer to entropy and temperature, respectively. Computations of the S and G quantities are carried out using the electronic, rotational, and vibrational parameters associated with the equilibrium structures according to the well-known thermochemical equations. A negative change in the Gibbs energy (free energy) represents a spontaneous interaction between the adsorbate molecule and adsorbent, which is desired in both drug delivery and drug sensor devices.

It is worth mentioning that a drug release from a carrier in the target cell is the most vital step in a drug delivery process. Owing to the excessive lactic production, a cancer cell is generally more acidic than normal cells ($pH < 7$) [105]. Thus, it is crucial to examine the performance of anticancer drug delivery systems in a low pH cancerous cell region for a better evaluation of the drug release performance of the nanostructure in the targeted region. This is well-known as the pH -dependent drug release mechanism [106].

Furthermore, the photochemical mechanism of light-triggered release from nanocarriers is also well known. Distinct wavelengths including ultraviolet (UV, 200–400 nm), visible (400–750 nm), and near-infrared (NIR, 780–1700 nm) lights, can be utilized to activate the light responsiveness [107]. Although the UV light is a relatively poor candidate due to its limited tissue penetration capacities and potentially carcinogenic effects under prolonged exposure, the NIR light has the advantages of lower phototoxicity, improved penetration depth in biological tissues, and reduced background signal. Thus, it is more suitable for biological applications. The NIR light is regarded as a transparent therapeutic window for light-activated delivery system *in vivo* due to its deep tissue penetration and minimum cellular damage [108]. The recovery time (Eq. (2)) could provide a theoretical estimation for light controlled release mechanism.

2.3 Electronic properties

The electronic properties investigation is usually performed using the HOMO-LUMO gap as a quantum descriptor, to establish correlation in various chemical and biochemical systems. The HOMO-LUMO gap E_g values are considered to explore the electronic properties and reactivities of the complexes formed upon interaction. This parameter is simply calculated by the following operational Eq. (4):

$$E_g = \varepsilon_{LUMO} - \varepsilon_{HOMO} \quad (4)$$

where ε_{HOMO} and ε_{LUMO} are the energies of the highest occupied molecular orbital (HOMO) and the lowest unoccupied molecular orbital (LUMO), respectively.

The electrical conductivity is exponentially related to the energy gap in a semiconductor material as follows (5):

$$\sigma = AT \frac{3}{2} e \left(-\frac{E_g}{2kT} \right) \quad (5)$$

where A (electrons/ $m^3K^{3/2}$) is a pre-factor constant, k is the Boltzmann's constant, and T is the absolute temperature. This equation has frequently been used and

previously demonstrated to yield results in agreement with experiment. The change in energy gap is a proper pointer for identification of the presence and attachment of a drug or biomolecule to a substrate.

Furthermore, the charge transfer between the adsorbate molecules and the adsorbent is generally performed through the natural bond orbital (NBO) or Hirshfeld population analyses. The amount of charge transfer plays an essential role in the development of a biosensor device. It helps determine the capability of a boron cluster in generating a detectable electrochemical signal on the presence of a biomolecule or a drug.

The electronic dipole moment is also an important issue for design of nanocarriers. The dissolvability of a nanostructure into a polar medium, such as an aqueous solution, can be explored using the dipole moment (μ). It plays a vital part in the design of a drug delivery device. A dipole moment enhancement is necessary for their solubility in a polar solvent. An increase in the hydrophilicity upon formation of the complex is a valuable factor for the efficient drug delivery system.

In summary, the structural, energetic, and electronic parameters necessary for the design of relevant materials are the basic molecular properties that can easily be determined using simple quantum chemical computations.

3. Boron clusters for biomedical applications

In this section, we discuss the studies reported on boron clusters in two separate categories, biosensors and drug delivery systems.

3.1 Biosensor applications

Kaur and Kumar [109] proposed a B_{40} -based biomarker for DNA sequencing from the results of DFT calculations using the Perdew-Burke-Ernzerhof (PBE) functional along with a double-zeta polarized basis set (DZP). These authors reported that all nucleobases are adsorbed on the surface of the B_{40} fullerene with the interaction energies of -18 , -15 , -16 , and -23 kcal/mol for adenine, thymine, cytosine, and guanine, respectively. No complex between the nucleobases and B_{40} was visualized. The analysis of transmission spectra, density of states, and eigenstates of the HOMO and LUMO revealed that all molecular junctions show transmission dominated by the HOMO. The highest energy gap was found in the adenine molecular junction, and this molecule gives the least value of current in comparison to the other molecular junctions.

Thus, by analysis of differential conductance curves for all the nucleobase- B_{40} junctions, it is deduced that the values of conductance are different from each other for all the junctions considered. This implies that B_{40} can appropriately be used as a biomarker for DNA sequencing applications, in predicting the sequence of nucleobases in a DNA strand. As another direct application, B_{40} can thus be employed as a multipurpose sensor for detection of the DNA nucleobases.

Kaur and coworkers explored in 2022 [110] the interaction of uracil on B_{40} utilizing DFT (PBE/DZP) and nonequilibrium Green's function regime computations. The physisorption phenomenon of the uracil molecule on the B_{40} surface is found, with an interaction distance of 2.38 \AA and an interaction energy of -19 kcal/mol. No orbital overlapping exists between uracil and B_{40} moiety according to an electron density analysis. The HOMO-LUMO energy gap of B_{40} decreases upon adsorption of uracil.

Although these authors suggested B_{40} as an effective biomarker to detect the presence of uracil molecule and thereby the mutations and cancerous tumors, the nature of the interaction is not well understood yet.

Rastgou et al. [111] examined the sensing ability of the quasi-planar B_{36} toward DNA nucleobases that might be used in a DNA sequencing device. The interaction energies for the most stable configuration of each complex were computed to be -57 , -43 , -38 , and -10 kcal/mol for adenine- B_{36} , guanine- B_{36} , cytosine- B_{36} , and thymine- B_{36} , respectively. It was found from DFT calculations using the B97D/6-31G(d) method that the cytosine interacts more considerably with the edge of B_{36} than other nucleobases, resulting in a large decrease in the energy gap, by 96% with respect to the isolated cluster. Such a decrease in the energy gap was observed at 36, 20, and 15% for thymine, adenine, and guanine, respectively. As a result, a change in conductivity could allow cytosine, followed by thymine, adenine, and guanine to be detected.

In particular, acetone ($CH_3C=OCH_3$) in the human breath exhaust is one of the commonly considered biomarkers for type-I as well as type-II diabetes. Yong and coworkers [112] studied in 2018 the potential capability of B_{40} and the doped $M@B_{40}$ ($M = Li$ and Ba) as acetone gas sensors using DFT calculations at the PBE/DZP level. The @ symbol stands hereafter for an encapsulation. The acetone molecule can easily adsorb on the B_{40} , $Li@B_{40}$, and $Ba@B_{40}$ clusters with interaction energies of -16 , -19 , and -8 kcal/mol, respectively. The recovery times were computed at 9.2 seconds for $Li@B_{40}$ and 1.2 seconds for $Ba@B_{40}$. Such a recovery time can be considered to be relatively long, as compared to a spectroscopic signal at the order of a microsecond, but it could be suitable for a sensor. The HOMO-LUMO gaps of $M@B_{40}$ again decrease upon acetone adsorption. Accordingly, the change in eclectic conductance of $Li@B_{40}$ or $Ba@B_{40}$ before and after the adsorption of acetone would be very distinctive, exhibiting the high sensitivity of $M@B_{40}$ for sensing acetone. Thus, the B_{40} and $M@B_{40}$ were introduced as highly sensitive molecular sensors for acetone detection, but the recovery time is relatively long at the order of a second.

The quasi-planar B_{36} was further explored for prospective sensing of the metronidazole (ML, cf. **Figure 4**) drug, which is an antibiotic drug with widespread usage but can cause unwanted hazardous effects on the human body. DFT calculations at the B3LYP-D3/6-31G(d) level demonstrated that ML interacts more strongly with B_{36} by its edge with an adsorption energy as high as -22 and -21 kcal/mol in both gaseous and aqueous phases, respectively. The change in Gibbs energy of -19 kcal/mol implies spontaneous adsorption. The decrease of 64% in the energy gap upon complexation is considerable, resulting in a substantial increase in the conductivity of the structure. The recovery time of the sensor was further found to be as 1.5 s for the most stable adsorption complex at room temperature. Again, such a time is rather long, but these results could be used to develop a boron-based sensor to detect the ML drug [113] in more appropriate time.

3.2 Drug delivery application

Solimannejad and coworkers investigated in 2018 [114] the possible complexes generated from the interaction between the amantadine drug (cf. **Figure 4**) and the bowl-like B_{30} using the DFT ω B97XD/6-31G(d, p) method in both gaseous and aqueous media. Amantadine drug has been used to treat the Parkinson's disease, influenza, or hepatitis for many years, even though in some cases it can cause some impairment of corneal endothelial function or corneal edema. The strongest interaction occurs between an edge boron atom of the B_{30} and an N atom of amantadine with binding

energy -46 and -53 kcal/mol in both gaseous and aqueous phases, respectively. The energy gap of the complex is remarkably reduced in both phases, with respect to the separated B_{30} . Thus B_{30} is quite sensitive to the presence of amantadine drug molecule, in such a way that it may be used in the sensor technology and possible drug delivery for amantadine for medicinal applications.

The interaction of fluorouracil (FU) with the quasi-planar B_{36} cluster was studied in 2017 [115] using the hybrid TPSSh functional with the $6-31 + G(d)$ basis set. The FU drug failed to generate any noticeable signal owing to the very weak interaction of this drug with the concave and convex surface of B_{36} ranging from -2 to -5 kcal/mol. Meanwhile, the FU drug remarkably interacts at its O atom site on the edge of the B_{36} with interaction energy of -24 and -27 kcal/mol in the gaseous and aqueous media, respectively (cf. **Figure 5**). The FU drug can also be detected by the B_{36} cluster with a noticeable signal owing to a significant decrease of 47% in the energy gap with respect to the free cluster. The dipole moment of FU- B_{36} complex was also observed as high as 17 and 36 Debye in the gas and water media, respectively, which indicates a large increase of the solubility in a polar medium.

Kamalinahad et al. performed in 2020 [116] a study on the interactions between sulfonamide (cf. **Figure 4**) and the B_{36} nanocluster through M06-2X/6-31G(d,p) computations. As a functional group, sulfonamide exists in several classes of drugs. Sulfonamide remarkably tends to adsorb via its oxygen atoms at the edge of B_{36} , alike FU drug, with interaction energy of -15 kcal/mol in both gaseous and aqueous

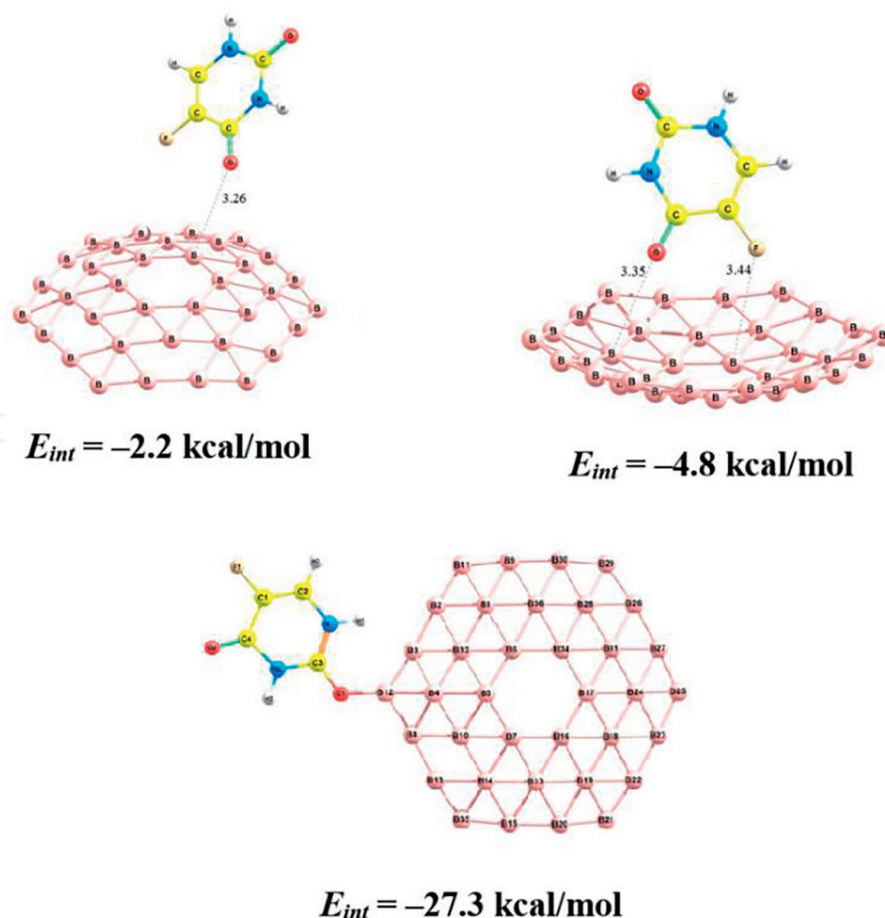


Figure 5. Configurations of the interaction in the FU- B_{36} complex. Values given are the interaction energies obtained by TPSSh/6-31G(d,p) computations.

media. The results illustrate that the edge B atoms are more reactive than the inner atoms toward the sulfonamide molecule leading to some large changes in its electronic features. The dipole moment of the complex increases to 13 Debye with respect to 4 Debye for the bare B_{36} cluster in aqueous medium. The high polarity together with appreciable adsorption energy suggested that these systems could be a vehicle for drug delivery.

Zheng et al. in 2020 [117] reported DFT computations at the PBE0/6-31 + G (d) level on the pristine and amino acid-functionalized C_4B_{32} fullerene as drug delivery agents for hydroxyurea (HU, cf. **Figure 4**) anticancer drug. These authors found that an alanine functionalization can significantly enhance the tendency of the carbon-doped C_4B_{32} cluster to the adsorption of HU. In this regard, the drug adsorption on the B atom of the clusters is more favorable than on the others. Indeed, the adsorption of HU drug on the cage part of the ala- C_4B_{32} isomers is stronger than that adsorbed on the alanine within a range of -16 to -19 kcal/mol in gas phase. Also, more negative adsorption occurs in aqueous medium, ranging from -20 to -23 kcal/mol, whose solubility can modify their interactions with the HU drug. The interactions between the HU drug and the clusters in the acidic condition become weak, and thereby the drug can faster be released from the carrier.

Yunyu and Jameh-Bozorgi [118] reported a DFT study at the PBE0/6-31 + G (d) level on the endohedral fullerenes $Li@C_4B_{32}$ and $Li@Si_4B_{32}$ as materials for drug delivery applications of the 6-thioguanine (TG) anticancer drug. These authors suggested the pristine and Li-encapsulation C_4B_{32} and Si_4B_{32} clusters as suitable for drug delivery applications. Calculated interaction energies were found to be -42 , -56 , -38 , and -43 kcal/mol for the TG/ C_4B_{32} , TG/ $Li@C_4B_{32}$, TG/ Si_4B_{32} , and TG/ $Li@Si_4B_{32}$ complexes, respectively. Such interaction energies are however quite large.

In fact, the strongest feature of the studied complexes bonding was found for TG/ $Li@C_4B_{32}$ with the maximum positive charge on B atoms, and the system with LUMOs orbitals distributed on B atoms that has been predicted as the most favorable site for the nucleophilic agents. Moreover, their computed ultraviolet-visible spectra reveal that the electronic spectra of the drug/cluster complexes exhibit a red shift toward higher wave lengths (lower transition energies). Furthermore, the interaction of TG with the clusters leads to narrower E_g values resulting again in an increase in conductivity. The effect of pH on the TG/ $Li@C_4B_{32}$ pointed out that the interaction energy in the acidic environment tends to decrease from 56 to 30 kcal/mol. Hence, the interactions between the drug and $Li@C_4B_{32}$ become again weaker in an acidic medium.

The alkali metal encapsulated fullerenes $M@C_4B_{32}$ with $M = Li, Na, \text{ and } K$ were considered as drug carrier agents for nitrosourea (NU) anticancer drug (cf. **Figure 4**) on the basis of calculations carried out using the PBE0/6-31 + G (d) approach [119]. A comparison between the interaction energies reveals that a potassium encapsulation inside C_4B_{32} can considerably enhance the tendency of cluster for adsorption of NU drug with an interaction energy of -37 kcal/mol. In this case, the interaction energy tends to increase to -41 kcal/mol in aqueous medium, and thereby the $K@C_4B_{32}$ cluster can increase its solubility and modify its interaction with the NU drug. The pH-dependent mechanism for drug release was also explored in which the proton (H^+) species attached to the NU. Results showed that the interaction between the NU drug and the $K@C_4B_{32}$ in an acidic environment is weaker with an interaction energy of -20 kcal/mol. Hence, the NU drug could better be released from a carrier in the targeted cancer cell in an acidic environment.

Furthermore, Luo and Gu [120] explored the ability of C_4B_{32} and Si_4B_{32} together with the Li encapsulated clusters for cisplatin (cf. **Figure 4**), using the PBE0/6-31 + G

(d) level leads to interaction energies of -28 , -12 , -18 , and -11 kcal/mol for the cisplatin/ C_4B_{32} , cisplatin/ $Li@C_4B_{32}$, cisplatin/ Si_4B_{32} , and cisplatin/ $Li@Si_4B_{32}$ complexes, respectively. The interaction distance for the cisplatin/ C_4B_{32} is relatively short (1.86 Å) in spite of relatively small interaction energy. Also, a blue shift toward lower wavelengths (larger transition energies) was observed from ultraviolet-visible spectra. Noticeably larger adsorption energies (more negative) are found in the solvent phase.

Sun and coworkers [121] explored the adsorption behavior of FU drug on B_{40} and some derivatives including MB_{39} and $M@B_{40}$ ($M = Mg, Al, Si, Mn, Cu, Zn$). These authors applied calculations using the B3LYP functional in conjunction with the SDD basis set with effective core potential for Cu, Mn, and Zn atoms and 6-31G(d) basis set for the other atoms. Accordingly, the FU drug prefers to attach to the corner boron atom of the B_{40} through one of its oxygen atoms, resulting in a strong polar covalent B–O bond. The corresponding interaction energy is calculated to be -11 kcal/mol. Additionally, the ΔH and ΔG values for the interaction of FU drug via B_{40} are both negative. Furthermore, they found that FU- B_{40} complex exhibits a much larger dipole moment of 9 Debye than those of 6 and 0 Debye for 5-FU and B_{40} , respectively, resulting in an increase in polarity for the whole system, and thus, enhancing the solubility of the resulting FU- B_{40} in an aqueous medium.

The drug release was also studied through a pH-dependent mechanism approach. The influence of pH on the FU- B_{40} complex was further examined by approaching a proton to the O atom of FU in complex. As seen in **Figure 6**, the distance between the O and B atoms greatly increases from 1.55 to 4.05 Å during the structural optimization. As a result, the interaction energy of FU- B_{40} severely decreases from -11 to -5 kcal/mol in the acidic environment, reflecting that the interaction between FU and B_{40} cluster is distinctly weakened under the attack of a single proton. Therefore, the FU drug can be released from the B_{40} carrier within the targeted tumor tissue where the medium is more acidic.

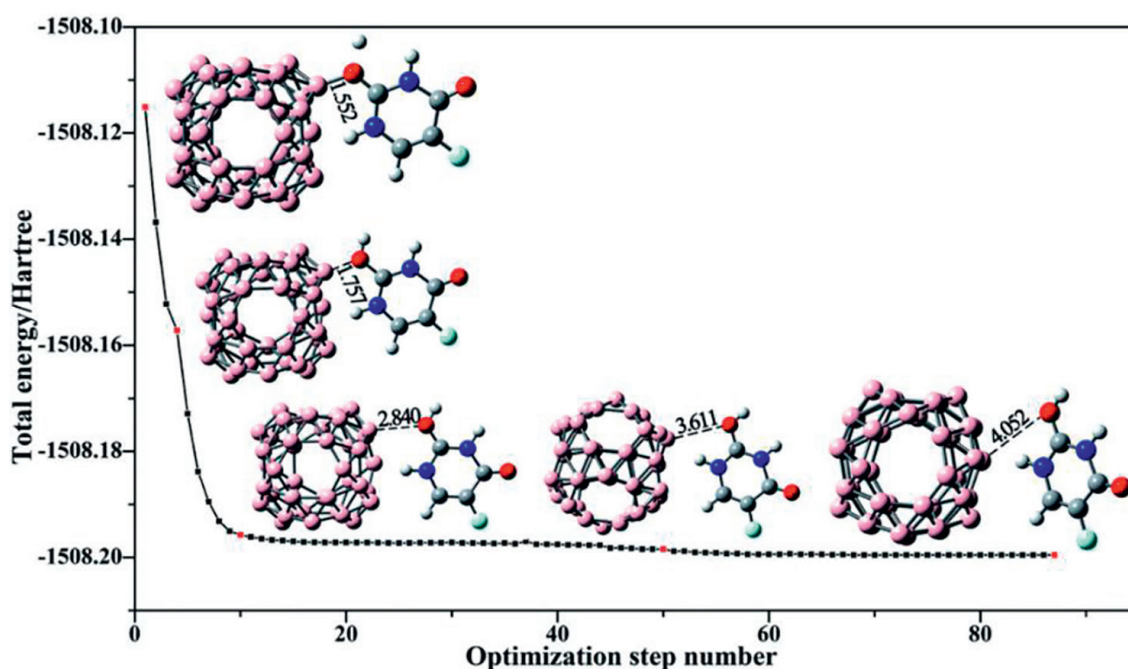


Figure 6.

Optimization process for the protonation of FU drug adsorbed on B_{40} cluster. The distances (in Å) between B and O atoms are also given. Figure reprinted with permission from ref. [121].

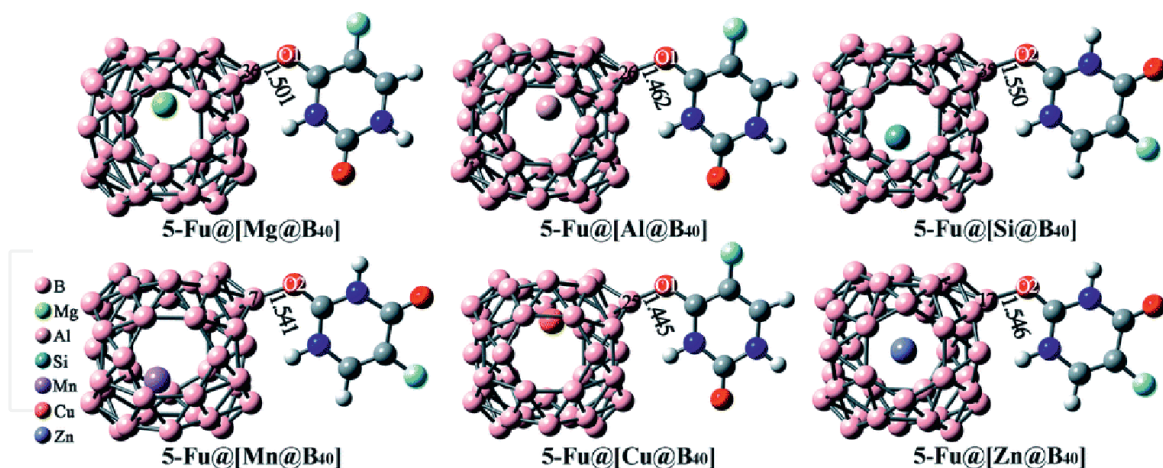


Figure 7. Optimized geometries of the most stable FU-[M@B₄₀] with M = Mg, Al, Si, Mn, Cu, and Zn complexes. The lengths of the newly formed bonds (in Å) are also given. Figure is reprinted with permission from ref. [121].

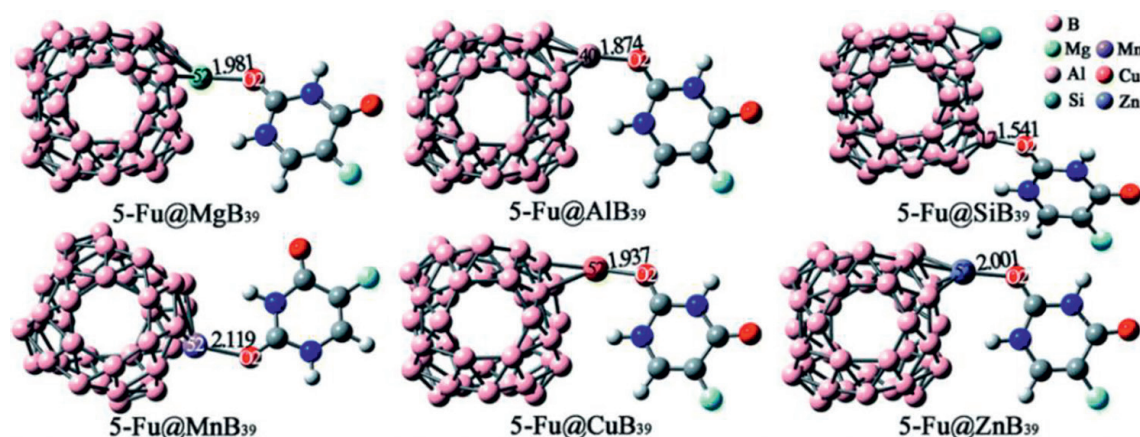


Figure 8. Optimized geometries of the most stable FU-B₃₉M (M = Mg, Al, Si, Mn, Cu, and Zn) complexes. The lengths of newly formed bonds (in Å) are also given. Figure is reprinted with permission from ref. [121].

Additionally, the substituent and encapsulation effects of Mg, Al, Si, Mn, Cu, and Zn atoms on the drug delivery performance of B₄₀ have been also explored. The FU oxygen atom tends to combine with MB₃₉ or M@B₄₀ cages, which are depicted in **Figures 7** and **8**, respectively. Interaction energies vary in the ordering (values in kcal/mol) -16 (FU-[Al@B₄₀]) -16 (FU-[Mg@B₄₀]) $>$ -15 (FU-[Cu@B₄₀]) $>$ -13 (FU-[Mn@B₄₀]) $>$ -12 (FU-[Zn@B₄₀]) $>$ -12 (FU-[Si@B₄₀]).

Meanwhile, the variation of interaction energies for the substituted complex is in the ordering of -30 (FU-B₃₉Al) -22 (FU-B₃₉Mg) $>$ -13 (FU-B₃₉Cu) $>$ -12 (FU-B₃₉Zn) $>$ -12 (FU-B₃₉Mn) $>$ -9 kcal/mol (FU-B₃₉Si). The absorption of FU on B₃₉M or M@B₄₀ cages is more favorable than pristine B₄₀ except for SiB₃₉. Therefore, the encapsulation and substitution of impurities can be regarded as an efficient approach to control and/or tune-up the interaction between the FU and B₄₀.

Sun and coworkers [122] explored the potential application of all-boron fullerene B₄₀ as a drug carrier for anti-cancer nitrosourea (NU, cf. **Figure 4**) by means of PBE0/6-31G (d, p) computations. The NU drug tends to combine with a corner B atom of the B₄₀ cage via its oxygen and nitrogen atoms with a moderate adsorption energy of -25 kcal/mol. The E_g value is decreased remarkably following adsorption

of NU drug because this raises its HOMO and reduces its LUMO level. However, a long recovery time of 52 seconds was predicted for the NU desorption process at 310 K, indicating quite long and difficult desorption of NU from B_{40} at human body temperature.

Moreover, B_{40} with a high drug loading capacity can simultaneously carry up to five NU drug molecules. Additionally, the substituent effect of C, N, Al, and Ga atoms on the drug delivery performance of this B_{40} cluster was investigated. The interaction energies vary in the sequence of -68 kcal/mol (NU- $B_{39}C$) $>$ -37 (NU- $B_{39}Al$) $>$ -19 (NU- $B_{39}Ga$) $>$ -18 (NU- $B_{39}N$). Also, the dipole moments were greatly enlarged from 1 to 6 Debye of $B_{39}M$ to 15–21 Debye of NU- $B_{39}M$ ($M = C, N, Al, \text{ and } Ga$). Therefore, it can be deduced that substitution of one boron atom of B_{40} by an exogenous atom indeed induces an obvious influence on the interaction between B_{40} and NU drug. As a result, the substituent effect of foreign atoms can be employed to modulate or tune up the drug adsorption performance of B_{40} cluster.

Interaction between the FU anticancer drug and the B_{40} fullerene was also investigated using the PBE-D/DZP level in both the gaseous and aqueous phases [123]. Results indicate that the FU molecule remarkably adsorbs on the top of B_{40} through its oxygen atom with moderate interaction energy of -24 kcal/mol (cf. **Figure 9**). The energy gap value of the FU- B_{40} complexes is relatively decreased by 21% as compared to the isolated B_{40} fullerene. The HOMO-LUMO gap of B_{40} amounts to 1.8 eV, which is reduced to 1.4 eV in FU- B_{40} . Thus, the adsorption of the FU molecule can be identified from electronic response, resulting from the decrease of electric conductivity. Furthermore, the FU molecule bears a Hirshfeld charge of 0.35 a.u. in complex, resulting in a charge-transfer complex, in which the charge is effectively transferred from the FU molecule to the B_{40} fullerene.

The capacity of B_{40} for carrying the FU drug was explored. All the six holes of B_{40} interact with FU molecules and the corresponding 6FU- B_{40} complexes in both gas phase and aqueous solution are achieved. The interaction energy was estimated to be -13 kcal/mol per FU drug molecule in both phases. Moreover, the energy gap is

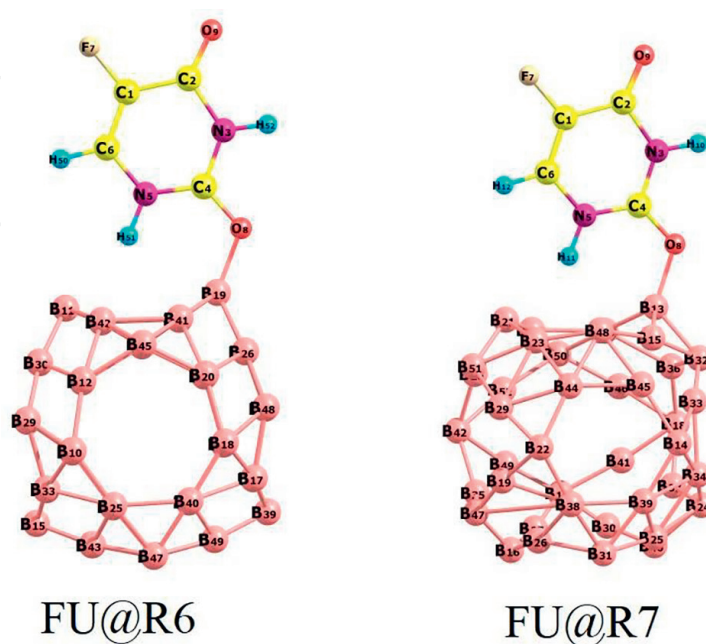


Figure 9. Optimized B_{40} -FU complexes. Figure is reprinted with permission from Ref. [123].

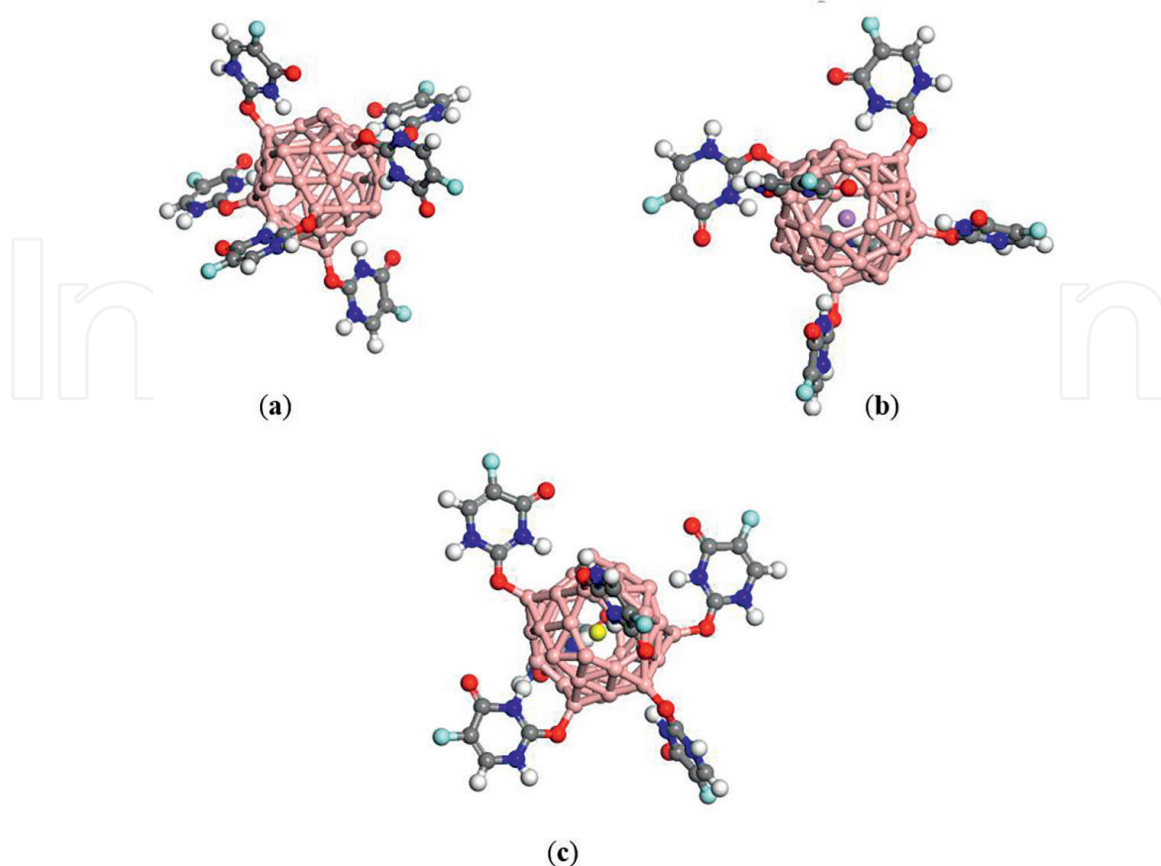


Figure 10. Optimized geometries of (a) 6FU- B_{40} , (b) $Na@B_{40}$ -6FU, and (c) $Ca@B_{40}$ -6FU complexes. Figure reprinted with permission from ref. [123].

distinctly decreased for this complex. The 6FU- B_{40} system has $E_g = 0.35$ eV in the gas phase and $E_g = 0.71$ eV in the aqueous phase.

The effect of Na and Ca encapsulation inside the B_{40} cluster on the FU adsorption behavior was also examined (cf. **Figure 10**). The interaction energy per FU molecule becomes now about -31 kcal/mol for 6FU- $Na@B_{40}$ and 6FU- $Ca@B_{40}$ systems in solution. Noticeably, the dipole moments enhance for the studied complexes in both phases. Further studies are needed to evaluate, in particular the recovery times, as to whether these fullerenes might behave as innovative boron-based candidates as drug delivery systems.

DFT (PBE-D/DZP) calculations were performed to investigate the interaction between the melphalan (MP; cf. **Figure 4**) as a chemotherapy medication and the bare as well as Na and Ca endohedral encapsulated B_{40} fullerenes ($M@B_{40}$ with $M = Na$ and Ca) [124]. The interaction energy of one MP drug with B_{40} was computed to be -15 kcal/mol. This interaction is a charge-transfer type occurring from the drug to the fullerene. The simultaneous adsorption of six MP molecules onto the fullerenes was also studied. An interaction energy of -4 kcal/mol per MP is obtained for 6MP- B_{40} system. Thus, it is deduced that the bare B_{40} fullerene suffers from a low adsorption energy per MP molecule in gas phase when it is fully loaded by MP drugs.

In order to improve the absorbency of B_{40} toward MP drug, the Na and Ca-encapsulated $Na@B_{40}$ and $Ca@B_{40}$ could yield some improvement (cf. **Figure 11**). The interaction energy per MP molecule increases now to -9 kcal/mol for the encapsulated fullerene in gas phase. Also, the dipole moment is enhanced in both gaseous

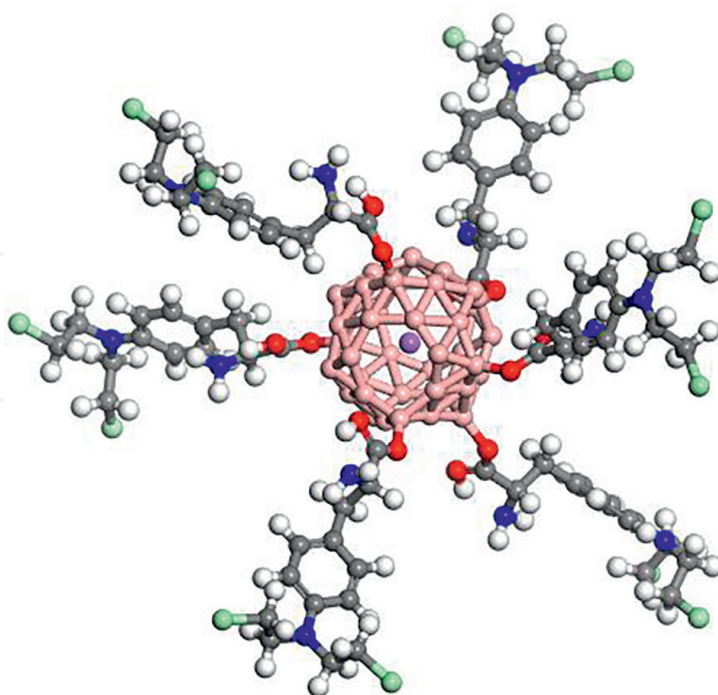


Figure 11.
Optimized geometries of the $M@B_{40}$ -6MP complexes.

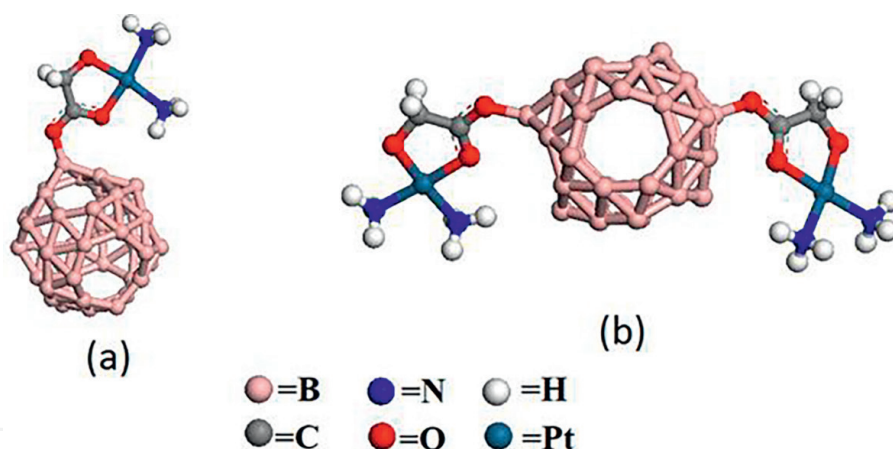


Figure 12.
Optimized geometries of (a) $NedaPt-B_{40}$ and (b) $2NedaPt-B_{40}$ complexes. Figure reprinted with permission from Ref. [125].

and aqueous phases for the resulting complexes, which is a crucial factor for the design of a drug carrier. The release of the MP drug from the carrier surface could be occurred through a pH -dependent mechanism.

The interaction between the nedaplatin anticancer drug (cf. **Figure 4**) with the B_{40} fullerene was also explored using PBE-D/DZP calculations in both vacuum and water mediums [125]. The nedaplatin molecule remarkably tends to adsorb on the top of B_{40} through its oxygen atom with an interaction energy of -18 kcal/mol. The adsorption of two nedaplatin molecules onto the fullerene holes has occurred with an interaction energy of -14 kcal/mol per drug molecule (cf. **Figure 12**).

Furthermore, reported results illustrate that the Li and Na encapsulation into B_{40} greatly increases the adsorption of nedaplatin in both the gaseous and solution

Adsorbate	Substrate	Level of theory	E_{int} (kcal/mol)	Ref.
Adenine	B ₄₀	PBE/DZP	-18	[111]
Thymine	B ₄₀	PBE/DZP	-15	[111]
Cytosine	B ₄₀	PBE/DZP	-16	[111]
Guanine	B ₄₀	PBE/DZP	-23	[111]
Uracil	B ₄₀	PBE/DZP	-19	[110]
Adenine	B ₃₆	B97D/6-31G(d)	-5	[109]
Thymine	B ₃₆	B97D/6-31G(d)	-10	[109]
Cytosine	B ₃₆	B97D/6-31G(d)	-38	[109]
Guanine	B ₃₆	B97D/6-31G(d)	-43	[109]
Acetone	B ₄₀	PBE/DNP	-15	[112]
Acetone	Li@B ₄₀	PBE/DNP	-19	[112]
Acetone	Ba@B ₄₀	PBE/DNP	-8	[112]
Metronidazole	B ₃₆	B3LYP-D3/6-31G(d)	-22	[113]
Amantadine	B ₃₀	ωB97XD/6-31G(d,p)	-46	[114]
Sulfonamide	B ₃₆	M06-2X/6-31G(d,p)	-15	[116]
5-Fluorouracil	B ₃₆	TPPSh/6-31 + G(d)	-24	[115]
Hydroxyurea	alanine-C ₄ B ₃₂	PBE0/6-31 + G(d)	-19	[117]
6-thioguanine	C ₄ B ₃₂	PBE0/6-31 + G(d)	-42	[118]
6-thioguanine	Si ₄ B ₃₂	PBE0/6-31 + G(d)	-56	[118]
6-thioguanine	Li@C ₄ B ₃₂	PBE0/6-31 + G(d)	-38	[118]
6-thioguanine	Li@Si ₄ B ₃₂	PBE0/6-31 + G(d)	-43	[118]
Nitrosourea	C ₄ B ₃₂	PBE0/6-31 + G(d)	-37	[119]
Cisplatin	C ₄ B ₃₂	PBE0/6-31 + G(d)	-28	[120]
Cisplatin	Si ₄ B ₃₂	PBE0/6-31 + G(d)	-18	[120]
Cisplatin	Li@C ₄ B ₃₂	PBE0/6-31 + G(d)	-12	[120]
Cisplatin	Li@Si ₄ B ₃₂	PBE0/6-31 + G(d)	-11	[120]
5-Fluorouracil	B ₄₀	B3LYP/6-31G(d)	-11	[121]
5-Fluorouracil	Al@B ₄₀	B3LYP/6-31G(d)	-15	[121]
5-Fluorouracil	Mg@B ₄₀	B3LYP/6-31G(d)	-15	[121]
5-Fluorouracil	Cu@B ₄₀	B3LYP/6-31G(d)	-15	[121]
5-Fluorouracil	Mn@B ₄₀	B3LYP/6-31G(d)	-13	[121]
5-Fluorouracil	Zn@B ₄₀	B3LYP/6-31G(d)	-12	[121]
5-Fluorouracil	Si@B ₄₀	B3LYP/6-31G(d)	-12	[121]
5-Fluorouracil	B ₃₉ Al	B3LYP/6-31G(d)	-29	[121]
5-Fluorouracil	B ₃₉ Mg	B3LYP/6-31G(d)	-22	[121]
5-Fluorouracil	B ₃₉ Cu	B3LYP/6-31G(d)	-13	[121]
5-Fluorouracil	B ₃₉ Zn	B3LYP/6-31G(d)	-12	[121]
5-Fluorouracil	B ₃₉ Mn	B3LYP/6-31G(d)	-12	[121]

5-Fluorouracil	B ₃₉ Si	B3LYP/6-31G(d)	-9	[121]
Nitrosourea	B ₄₀	PBE0/6-31G(d,p)	-25	[122]
Nitrosourea	B ₃₉ C	PBE0/6-31G(d,p)	-36	[122]
Nitrosourea	B ₃₉ Al	PBE0/6-31G(d,p)	-19	[122]
Nitrosourea	B ₃₉ Ga	PBE0/6-31G(d,p)	-18	[122]
5-Fluorouracil	B ₄₀	PBE-D/DNP	-13	[123]
5-Fluorouracil	Na@B ₄₀	PBE-D/DNP	-16	[123]
5-Fluorouracil	Ca@B ₄₀	PBE-D/DNP	-17	[123]
Melphalan	B ₄₀	PBE-D/DNP	-3	[124]
Melphalan	Na@B ₄₀	PBE-D/DNP	-8	[124]
Melphalan	Ca@B ₄₀	PBE-D/DNP	-9	[124]
Nedaplatin	B ₄₀	PBE-D/DNP	-13	[125]
Nedaplatin	Li@B ₄₀	PBE-D/DNP	-20	[125]
Nedaplatin	Na@B ₄₀	PBE-D/DNP	-18	[125]

Table 1.

Summary of the interaction energies of boron-based clusters with bio-molecules considered in biomedical applications.

phases. The adsorption energy per nedaplatin molecule is about -28 kcal/mol for both Li@B₄₀ and Na@B₄₀ fullerene in aqueous solution, which is greater than that of the bare B₄₀ fullerene, which is not favorable to be used.

4. Concluding remarks

Table 1 summarizes the reported interaction energies of boron-based clusters with the bio-molecules considered. Interaction energy constitutes the main parameter to evaluate the suitability of a carrier molecule for biomedical applications. Although the number of studies is rather limited, an analysis of these theoretical results suggests that boron-based clusters deserve to be regarded as promising candidates for the bio-sensing and drug delivery-related applications.

A large interaction energy indicates a stable complex, but it invariably causes a longer recovery time, which is not a good factor for drug release or for refreshing a biosensor. Thus, a semi-chemisorption with an effective recovery time (less than 1 second) is more favorable for biomedical applications. Based on Eq. (2), the recovery of a biomedical agent from a typical carrier surface is estimated to be short in the range 0.03–0.06 microsecond for NIR light with the typical interaction energy of -10 kcal/mol at 310 K of the human body. Also, it amounts to 0.3–0.7 second for interaction energies of -20 kcal/mol, which seems to be usable for an appropriate biosensor [107].

The recovery time exponentially increases by an enhancement of interaction energy. According to **Table 1**, most of the reported interaction energies are smaller than -20 kcal/mol, with an expected error margin of ± 3 kcal/mol for DFT computations, which provide suitable recovery times at human body temperature in the range of NIR light.

In spite of the frequent claims of many authors in reported theoretical studies, some systems are not suitable due to a long recovery time (in the order of second or even longer). For example, in the aforementioned condition, B_{36} suffers from long recovery time for sensing cytosine and guanine; similarly, C_4B_{32} suffers from long recovery time for detecting 6-thioguanine, nitrosourea, and cisplatin drugs.

Noticeably, the release mechanism of drug is also a crucial factor, which should be understood for a better design of a drug delivery system, in addition to suitable recovery time. Such studies are yet to be carried out.

In summary, from a theoretical viewpoint, boron-based clusters having some unique structural and electronic properties provide us with great potential in biomedical applications. Quantum chemical calculations can further assist experimental researchers in the understanding of these systems from the molecular insights at low cost but with much detail and substantial accuracy.

Acknowledgements

The work of LVD and MTN is funded by VinGroup (Vietnam) and supported by VinGroup Innovation Foundation (VinIF) under project code VinIF_2020_DA21. LVD is thankful to the Van Lang University.

Conflict of interest

The authors declare no conflict of interest.

IntechOpen

IntechOpen

Author details

Ehsan Shakerzadeh^{1*}, Elham Tahmasebi¹, Long Van Duong^{2,3}
and Minh Tho Nguyen^{4,5*}

1 Chemistry Department, Faculty of Science, Shahid Chamran University of Ahvaz, Ahvaz, Iran

2 Laboratory for Computational Molecular and Materials Sciences, Science and Technology Advanced Institute, Van Lang University, Ho Chi Minh City, Vietnam


3 Faculty of Applied Technology, School of Engineering and Technology, Van Lang University, Ho Chi Minh City, Vietnam

4 Institute for Computational Science and Technology (ICST), Ho Chi Minh City, Vietnam

5 Department of Chemistry, KU Leuven, Leuven, Belgium

*Address all correspondence to: e.shakerzadeh@scu.ac.ir and tho.nm@icst.org.vn

IntechOpen

© 2022 The Author(s). Licensee IntechOpen. This chapter is distributed under the terms of the Creative Commons Attribution License (<http://creativecommons.org/licenses/by/3.0>), which permits unrestricted use, distribution, and reproduction in any medium, provided the original work is properly cited. 

References

- [1] Alphandéry E. Ultrasound and nanomaterial: An efficient pair to fight cancer. *Journal of Nanobiotechnology*. 2022;**20**:139. DOI: 10.1186/s12951-022-01243-w
- [2] Jedla MR, Koneru B, Franco A, Rangappa D, Banerjee P. Recent developments in nanomaterials based adsorbents for water purification techniques. *Biointerface Research and Applied Chemistry*. 2022;**12**:5821-5835. DOI: 10.33263/BRIAC125.58215835
- [3] Hu ZT, Chen Y, Fei YF, Loo SL, Chen G, Hu M, et al. An overview of nanomaterial-based novel disinfection technologies for harmful microorganisms: Mechanism, synthesis, devices and application. *Science Total Environment*. 2022;**837**:155720. DOI: 10.1016/j.scitotenv.2022.155720
- [4] Yuan F, Xia Y, Lu Q, Xu Q, Shu Y, Hu X. Recent advances in inorganic functional nanomaterials based flexible electrochemical sensors. *Talanta*. 2022;**244**:123419. DOI: 10.1016/j.talanta.2022.123419
- [5] Rahman H, Hossain MR, Ferdous T. The recent advancement of low-dimensional nanostructured materials for drug delivery and drug sensing application: A brief review. *Journal of Molecular Liquids*. 2020;**320**:114427. DOI: 10.1016/j.molliq.2020.114427
- [6] Zhu X, Chen H, Zhou Y, Wu J, Ramakrishna S, Peng X, et al. Recent advances in biosensors for detection of exosomes. *Curr Opin Biomed Eng*. 2021;**18**:100280. DOI: 10.1016/j.cobme.2021.100280
- [7] Dyussebayev K, Sambasivam P, Bar I, Brownlie JC, Shiddiky MJA, Ford R. Biosensor Technologies for early detection and quantification of plant pathogens. *Frontiers in Chemistry*. 2021;**9**:636245. DOI: 10.3389/fchem.2021.636245
- [8] Eivazzadeh-Keihan R, Bahojb Noruzi E, Chidar E, Jafari M, Davoodi F, Kashtiaray A, et al. Applications of carbon-based conductive nanomaterials in biosensors. *Chemical Engineering Journal*. 2022;**442**:136183. DOI: 10.1016/j.cej.2022.136183
- [9] Machado M, Oliveira AML, Silva GA, Bitoque DB, Ferreira JT, Pinto LA, et al. Graphene biosensors—A molecular approach. *Nanomaterials*. 2022;**12**:1624. DOI: 10.3390/nano12101624
- [10] Pourmadadi M, Dinani HS, Tabar FS, Khassi K, Janfaza S, Tasnim N, et al. Properties and applications of graphene and its derivatives in biosensors for Cancer detection: A comprehensive review. *Biosensors*. 2022;**12**:269. DOI: 10.3390/bios12050269
- [11] Chao L, Liang Y, Hu X, Shi H, Xia T, Zhang H, et al. Recent advances in field effect transistor biosensor technology for cancer detection: A mini review. *Journal of Physics D: Applied Physics*. 2022;**55**:153001. DOI: 10.1088/1361-6463/ac3f5a
- [12] Liu J, Yan L, He S, Hu J. Engineering DNA quadruplexes in DNA nanostructures for biosensor construction. *Nano Research*. 2022;**15**:3504-3513. DOI: 10.1007/s12274-021-3869-y
- [13] Deng Y, Sun Z, Wang L, Wang M, Yang J, Li G. Biosensor-based assay of exosome biomarker for early diagnosis of cancer. *Frontiers in Medicine*.

2022;**16**:157-175. DOI: 10.1007/s11684-021-0884-z

[14] Yang YJ, Gao ZF. Superwetable biosensor for disease biomarker detection. *Frontiers in Bioengineering and Biotechnology*. 2022;**10**:872984. DOI: 10.3389/fbioe.2022.872984

[15] Chupradit S, Jasim SA, Bokov D, Mahmoud MZ, Roomi AB, Hachem K, et al. Recent advances in biosensor devices for HER-2 cancer biomarker detection. *Analytical Methods*. 2022;**14**:1301-1310. DOI: 10.1039/d2ay00111j

[16] Jiang C, Mu X, Du B, Tong Z. A review of electrochemical biosensor application in the detection of the SARS-CoV-2. *Micro Nano Letters*. 2022;**17**:49-58. DOI: 10.1049/mna2.12101

[17] Breshears LE, Nguyen BT, Mata Robles S, Wu L, Yoon JY. Biosensor detection of airborne respiratory viruses such as SARS-CoV-2. *SLAS Technology*. 2022;**27**:4-17. DOI: 10.1016/j.slast.2021.12.004

[18] El-Sherif DM, Abouzid M, Gaballah MS, Ahmed AA, Adeel M, Sheta SM. New approach in SARS-CoV-2 surveillance using biosensor technology: A review. *Environmental Science and Pollution Research*. 2022;**29**:1677-1695. DOI: 10.1007/s11356-021-17096-z

[19] Shobana MK. Nanoferrites in biosensors – A review. *Materials Science & Engineering, B: Solid-State Materials for Advanced Technology*. 2021;**272**:115344. DOI: 10.1016/j.mseb.2021.115344

[20] Aljuffali IA, Fang CL, Chen CH, Fang JY. Nanomedicine as a strategy for natural compound delivery to prevent and treat cancers. *Current Pharmaceutical Design*.

2016;**22**:4219-4231. DOI: 10.2174/1381612822666160620072539

[21] Edis Z, Wang J, Waqas MK, Ijaz M, Ijaz M. Nanocarriers-mediated drug delivery Systems for Anticancer Agents: An overview and perspectives. *International Journal of Nanomedicine*. 2021;**16**:1313-1330. DOI: 10.2147/IJN.S289443

[22] Din FU, Aman W, Ullah I, Qureshi OS, Mustapha O, Shafique S, et al. Effective use of nanocarriers as drug delivery systems for the treatment of selected tumors. *International Journal of Nanomedicine*. 2017;**12**:7291-7309. DOI: 10.2147/IJN.S146315

[23] Alotaibi BS, Buabeid M, Ibrahim NA, Kharaba ZJ, Ijaz M, Noreen S, et al. Potential of nanocarrier-based drug delivery Systems for Brain Targeting: A current review of literature. *International Journal of Nanomedicine*. 2021;**16**:7517-7533. DOI: 10.2147/IJN.S33365

[24] Entezar-Almahdi E, Mohammadi-Samani S, Tayebi L, Farjadian F. Recent advances in designing 5-fluorouracil delivery systems: A stepping Stone in the safe treatment of colorectal Cancer. *International Journal of Nanomedicine*. 2020;**15**:5445-5458. DOI: 10.2147/IJN.S257700

[25] Wang LM, Wang YT, Yang WX. Engineered nanomaterials induce alterations in biological barriers: Focus on paracellular permeability. *Nanomedicine*. 2021;**16**:2725-2741. DOI: 10.2217/nnm-2021-0165

[26] Liu H, Zhang R, Zhang D, Zhang C, Zhang Z, Fu X, et al. Cyclic RGD-decorated liposomal gossypol AT-101 targeting for enhanced antitumor effect. *International Journal of Nanomedicine*. 2022;**17**:228-244. DOI: 10.2147/IJN.S341824

- [27] Li X, Golberg D. Chapter 5 - boron nitride nanotubes as drug carriers. In: Ciofani G, Mattoli VBTBNN in N, editors. *Micro and Nano Technologies*. Boston: William Andrew Publishing; 2016. p. 79-94. DOI:10.1016/B978-0-323-38945-7.00005-5
- [28] Lan HR, Wu ZQ, Zhang LH, Jin KT, Wang SB. Nanotechnology assisted chemotherapy for targeted Cancer treatment: Recent advances and clinical perspectives. *Current Topics in Medicinal Chemistry*. 2020;**20**:2442-2458. DOI: 10.2174/1568026620666200722110808
- [29] Kenchegowda M, Rahamathulla M, Hani U, Begum MY, Guruswamy S, Osmani RAM, et al. Smart nanocarriers as an emerging platform for cancer therapy: A review. *Molecules*. 2020;**21**:146
- [30] Rahimi R, Solimannejad M. First-principles survey on the pristine BC₂N monolayer as a promising vehicle for delivery of β -lapachone anticancer drug. *Journal of Molecular Liquids*. 2021;**321**:114917. DOI: 10.1016/j.molliq.2020.114917
- [31] Sun X, Wan X, Li G, Yu J, Vahabi V. Amantadine antiparkinsonian drug adsorption on the AlN and BN nanoclusters: A computational study. *Physics Letters A*. 2020;**384**:126128. DOI: 10.1016/j.physleta.2019.126128
- [32] Rahimi R, Solimannejad M, Ehsanfar Z. Potential application of XC₃ (X=B, N) nanosheets in drug delivery of hydroxyurea anticancer drug: A comparative DFT study. *Molecular Physics*. 2022;**120**:6. DOI: 10.1080/00268976.2021.2014587
- [33] Zhu H, Zhao C, Cai Q, Fu X, Sheykhahmad FR. Adsorption behavior of 5-aminosalicylic acid drug on the B₁₂N₁₂, AlB₁₁N₁₂ and GaB₁₁N₁₂ nanoclusters: A comparative DFT study. *Inorganic Chemistry Communications*. 2018;**79**:223-229. DOI: 10.1016/j.inoche.2020.107808
- [34] Onori S, Alipour E. A computational study on the cisplatin drug interaction with boron nitride nanocluster. *Journal of Molecular Graphics & Modelling*. 2018;**79**:223-229. DOI: 10.1016/j.jmngm.2017.12.007
- [35] Balali E, Davatgaran S, Sheikhi M, Shahab S, Kaviani S. Adsorption of doxepin drug on the surface of B₁₂N₁₂ and Al₁₂N₁₂ nanoclusters: DFT and TD-DFT perspectives. *Main Group Chemistry*. 2022;**21**:69-84. DOI: 10.3233/MGC-210083
- [36] Ganji MD, Yazdani H, Mirnejad A. B₃₆N₃₆ fullerene-like nanocages: A novel material for drug delivery. *Physica E Low-Dimensional System Nanostructures*. 2010;**42**:2184-2189. DOI: 10.1016/j.physe.2010.04.018
- [37] Shabani M, Ghiasi R, Zare K, Fazaeli R. Quantum chemical study of interaction between Titanocene dichloride anticancer drug and Al₁₂N₁₂ Nano-cluster. *Russian Journal of Inorganic Chemistry*. 2020;**65**:1726-1734. DOI: 10.1134/S0036023620110169
- [38] Yuan J, Mohamadi A. Study the adsorption process of 5-fluorouracil drug on the pristine and doped graphdiyne nanosheet. *Journal of Molecular Modeling*. 2021;**27**:32. DOI: 10.1007/s00894-020-04629-5
- [39] Abd El-Mageed HR, Abbas HS. Adsorption behavior of mercaptopurine and 6-thioguanine drugs on the B₁₂N₁₂, AlB₁₁N₁₂ and GaB₁₁N₁₂ nanoclusters, a comparative DFT study. *Journal of Biomolecular Structure & Dynamics*. 2021;**12**:1-20. DOI: 10.1080/07391102.2021.1930163

- [40] Yang Y, Ostadhosseini N. A theoretical investigation on the mercaptopurine drug interaction with boron nitride nanocage: Solvent and density functional effect. *Physica E Low-Dimensional System Nanostructures*. 2021;**125**:114337. DOI: 10.1016/j.physe.2020.114337
- [41] Rahimi R, Solimannejad M, Farghadani M. Adsorption of chloroquine and hydroxychloroquine as potential drugs of SARS-CoV-2 infection on BC₃ nanosheets: A DFT study. *New Journal of Chemistry*. 2021;**45**:17976-17983. DOI: 10.1039/D1NJ03084A
- [42] Khezri B, Maskanati M, Ghanemnia N, Shabani Gokeh M, Rezaei S, Chang L. Efficient detection of thioguanine drug using boron nitride nanocage: DFT outlook of solvent effect and AIM analysis. *Inorganic Chemistry Communications*. 2021;**134**:109015. DOI: 10.1016/j.inoche.2021.109015
- [43] Shakerzadeh E. Chapter 4 - theoretical investigations of interactions between boron nitride nanotubes and drugs. In: Ciofani G, Mattoli VBTBNN in N, editors. *Micro and Nano Technologies*. Boston: William Andrew Publishing; 2016. p. 59-77. DOI:10.1016/B978-0-323-38945-7.00004-3
- [44] Golipour-Chobar E, Salimi F, Ebrahimzadeh RG. Boron nitride nanocluster as a carrier for lomustine anticancer drug delivery: DFT and thermodynamics studies. *Monatshefte für Chemie*. 2020;**151**:309-318. DOI: 10.1007/s00706-020-02564-y
- [45] El-Mageed HRA, Mustafa FM, Abdel-Latif MK. Boron nitride nanoclusters, nanoparticles and nanotubes as a drug carrier for isoniazid anti-tuberculosis drug, computational chemistry approaches. *Journal of Biomolecular Structure & Dynamics*. 2022;**40**:226-235. DOI: 10.1080/07391102.2020.1814871
- [46] Stone FGA. Chemical reactivity of the boron hydrides and related compounds. In: Emeleus HJ, Sharpe AG, editors. *Academic Press, Advances in Inorganic Chemistry and Radiochemistry*. 1960. pp. 279-313
- [47] Tao Y, Wu X, Zhang D. Synthesis and solar blind photosensitivity of crystalline boron nanowires. *Nanotechnology*. 2022;**33**:235601. DOI: 10.1088/1361-6528/ac56f5
- [48] Wu Y, Li Y, Chen H, Sun Z, Wang N, Qin J, et al. Growth of single crystalline boron nanotubes in a Cu alloy. *Crystal Engineering Communication*. 2017;**19**:4510-4518. DOI: 10.1039/c7ce00818j
- [49] Xu J, Chang Y, Gan L, Ma Y, Zhai T. Ultrathin single-crystalline boron nanosheets for enhanced electro-optical performances. *Advancement of Science*. 2015;**2**:1500023. DOI: 10.1002/advs.201500023
- [50] Mannix AJ, Zhou XF, Kiraly B, Wood JD, Alducin D, Myers BD, et al. Synthesis of borophenes: Anisotropic, two-dimensional boron polymorphs. *Science*. 2015;**350**:1513-1516. DOI: 10.1126/science.aad1080
- [51] Feng B, Zhang J, Zhong Q, Li W, Li S, Li H, et al. Experimental realization of two-dimensional boron sheets. *Nature Chemistry*. 2016;**8**:563-568. DOI: 10.1038/nchem.2491
- [52] Otten CJ, Lourie OR, Yu MF, Cowley JM, Dyer MJ, Ruoff RS, et al. Crystalline boron nanowires. *Journal of the American Chemical Society*. 2002;**124**:4564-4565. DOI: 10.1021/ja017817s

- [53] Xu TT, Zheng JG, Wu N, Nicholls AW, Roth JR, Dikin DA, et al. Crystalline boron nanoribbons: Synthesis and characterization. *Nano Letters*. 2004;**4**:963-968. DOI: 10.1021/nl0498785
- [54] Tai G, Hu T, Zhou Y, Wang X, Kong J, Zeng T, et al. Synthesis of atomically thin boron films on copper foils. *Angewandte Chemie, International Edition*. 2015;**54**:15473-15477. DOI: 10.1002/anie.201509285
- [55] Wu R, Drozdov IK, Eltinge S, Zahl P, Ismail-Beigi S, Božović I, et al. Large-area single-crystal sheets of borophene on Cu (111) surfaces. *Nature Nanotechnology*. 2019;**14**:44-49. DOI: 10.1038/s41565-018-0317-6
- [56] Liu F, Shen C, Su Z, Ding X, Deng S, Chen J, et al. Metal-like single crystalline boron nanotubes: Synthesis and in situ study on electric transport and field emission properties. *Journal of Materials Chemistry*. 2010;**20**:2197-2205. DOI: 10.1039/b919260c
- [57] Meng XM, Hu JQ, Jiang Y, Lee CS, Lee ST. Boron nanowires synthesized by laser ablation at high temperature. *Chemical Physics Letters*. 2003;**370**:825-828. DOI: 10.1016/S0009-2614(03)00202-1
- [58] Van DL, Mai DTT, Pham-Ho MP, Nguyen MT. A theoretical approach to the role of different types of electrons in planar elongated boron clusters. *Physical Chemistry Chemical Physics*. 2019;**21**:13030-13039. DOI: 10.1039/C9CP00737G
- [59] Tam NM, Duong LV, Pham HT, Nguyen MT, Pham-Ho MP. Effects of single and double nickel doping on boron clusters: Stabilization of tubular structures in B_nNi_m , ($n = 2-22$, $m = 1, 2$). *Physical Chemistry Chemical Physics*. 2019;**21**:8365-8375. DOI: 10.1039/C9CP00762H
- [60] Dong X, Jalife S, Vásquez-Espinal A, Barroso J, Orozco-Ic M, Ravell E, et al. Li_2B_{24} : The simplest combination for a three-ring boron tube. *Nanoscale*. 2019;**55**:7490-7493. DOI: 10.1039/C9CC03732B
- [61] Liang WY, Barroso J, Jalife S, Orozco-Ic M, Zarate X, Dong X, et al. $B_{10}M_2$ ($M = Rh, Ir$): Finally a stable boron-based icosahedral cluster. *Chemical Communications*. 2019;**55**:7490-7493. DOI: 10.1039/C9CC03732B
- [62] Pan S, Barroso J, Jalife S, Heine T, Asmis KR, Merino G. Fluxional boron clusters: From theory to reality. *Accounts of Chemical Research*. 2019;**52**:2732-2744. DOI: 10.1021/acs.accounts.9b00336
- [63] Li Q, Zhao Y, Xu W, Li N. Structure and stability of B_8 clusters. *International Journal of Quantum Chemistry*. 2005;**101**:219-229. DOI: 10.1002/qua.20290
- [64] Dong X, Jalife S, Vásquez-Espinal A, Ravell E, Pan S, Cabellos JL, et al. Li_2B_{12} and Li_3B_{12} : Prediction of the smallest tubular and cage-like boron structures. *Angewandte Chemie, International Edition*. 2018;**57**:4627-4631. DOI: 10.1002/anie.201800976
- [65] Pham HT, Van DL, Pham BQ, Nguyen MT. The 2D-to-3D geometry hopping in small boron clusters: The charge effect. *Chemical Physics Letters*. 2013;**577**:32-37. DOI: 10.1016/j.cplett.2013.05.041
- [66] Tam NM, Pham HT, Duong LV, Pham-Ho MP, Nguyen MT. Fullerene-like boron clusters stabilized by an endohedrally doped iron atom: B_nFe with $n = 14, 16, 18$ and 20 . *Physical Chemistry*

Chemical Physics. 2015;**17**:3000-3003.
DOI: 10.1039/C4CP04279D

[67] Mai DTT, Duong LV, Tai TB, Nguyen MT. Electronic structure and thermochemical parameters of the silicon-doped boron clusters B_nSi , with $n=8-14$, and their anions. *The Journal of Physical Chemistry. A*. 2016;**120**: 3623-3633. DOI: 10.1021/acs.jpca.6b00847

[68] Duong LV, Si NT, Hung NP, Nguyen MT. The binary boron lithium clusters $B_{12}Li_n$ with $n=1-14$: In search for hydrogen storage materials *Phys. Chemistry and Chemical Physics*. 2021;**23**:24866. DOI: 10.1039/D1CP03682C

[69] Pham-Ho MP, Tan Pham H, Nguyen MT. Boron teetotum: Metallic $[Ti(B_6C_xN_y)]^q$ and bimetallic $[Ti_2(B_6C_xN_y)]^q$ nine-membered heterocycles with $x+y=3$ and $-1 \leq q \leq 3$. *The Journal of Physical Chemistry. A*. 2018;**122**: 6196-6205. DOI: 10.1021/acs.jpca.8b02713

[70] Pham HT, Muya JT, Buendía F, Ceulemans A, Nguyen MT. Formation of the quasi-planar B_{50} boron cluster: Topological path from B_{10} and disk aromaticity. *Physical Chemistry Chemical Physics*. 2019;**21**:7039-7044. DOI: 10.1039/C9CP00735K

[71] Pham HT, Nguyen MT. Formation of a bi-rhodium boron tube Rh_2B_{18} and its great CO_2 capture ability. *Physical Chemistry Chemical Physics*. 2018;**20**:26072-26082. DOI: 10.1039/C8CP03584A

[72] Duong LV, Pham HT, Tam NM, Nguyen MT. A particle on a hollow cylinder: The triple ring tubular cluster B_{27}^+ . *Physical Chemistry Chemical Physics*. 2014;**16**:19470-19478. DOI: 10.1039/C4CP01996B

[73] Tai TB, Nguyen MT. Electronic structure and photoelectron spectra of B_n

with $n=26-29$: An overview of structural characteristics and growth mechanism of boron clusters. *Physical Chemistry Chemical Physics*. 2015;**17**:13672-13679. DOI: 10.1039/c5cp01851j

[74] Tai TB, Van DL, Pham HT, Mai DTT, Nguyen MT. A disk-aromatic bowl cluster B_{30} : Toward formation of boron buckyballs. *Chemical Communications*. 2014;**50**:1558-1560. DOI: 10.1039/C3CC48392D-

[75] Pham HT, Duong LV, Tam NM, Pham-Ho MP, Nguyen MT. The boron conundrum: Bonding in the bowl B_{30} and B_{36} , fullerene B_{40} and triple ring B_{42} clusters. *Chemical Physics Letters*. 2014;**608**:295-302. DOI: 10.1016/j.cplett.2014.05.069

[76] Piazza ZA, Hu HS, Li WL, Zhao YF, Li J, Wang LS. Planar hexagonal B_{36} as a potential basis for extended single-atom layer boron sheets. *Nature Communications*. 2014;**5**:3113. DOI: 10.1038/ncomms4113

[77] Bai H, Ma M, Zuo J, Zhang QF, Bai B, Cao H, et al. Recyclable and superior selective CO_2 adsorption of C_4B_{32} and $Ca@C_4B_{32}$: A new category of perfect cubic heteroborospherenes. *Physical Chemistry Chemical Physics*. 2019;**21**:15541-15550. DOI: 10.1039/c9cp02380a

[78] Liu P, Zhang Y, Liu F, Zhou D. Li decorated heteroborospherene C_4B_{32} as high capacity and reversible hydrogen storage media: A DFT study. *International Journal of Hydrogen Energy*. 2022;**47**:11948-11954. DOI: 10.1016/j.ijhydene.2022.01.208

[79] Zhai HJ, Zhao YF, Li WL, Chen Q, Bai H, Hu HS, et al. Observation of an all-boron fullerene. *Nature Chemistry*. 2014;**6**:727-731. DOI: 10.1038/nchem.1999

- [80] Shakerzadeh E, Biglari Z, Tahmasebi E. M@B₄₀ (M=Li, Na, K) serving as a potential promising novel NLO nanomaterial. *Chemical Physics Letters*. 2016;**654**:76-80. DOI: 10.1016/j.cplett.2016.05.016
- [81] Shakerzadeh E, Kazemimoghadam F. Magnesianation of bare and halides encapsulated B₄₀ fullerenes for their potential application as promising anode materials for Mg-ion batteries. *Applied Surface Science*. 2021;**538**:148060. DOI: 10.1016/j.apsusc.2020.148060
- [82] Kaur R, Kaur J. The electronic transport properties of B₄₀ fullerenes with chalcogens as anchor atoms. *Journal of Molecular Modeling*. 2017;**23**:351. DOI: 10.1007/s00894-017-3520-8
- [83] Shakerzadeh E, Yousefizadeh M, Bamdad M. Electronic and nonlinear optical features of first row transition metals-decorated all-boron B₄₀ fullerene: A promising route to remarkable electro-optical response. *Inorganic Chemistry Communications*. 2020;**112**:107692. DOI: 10.1016/j.inoche.2019.107692
- [84] Yang Y, Zhang Z, Penev ES, Yakobson BI. B₄₀ cluster stability, reactivity, and its planar structural precursor. *Nanoscale*. 2017;**9**:1805-1810. DOI: 10.1039/c6nr09385j
- [85] Kaur H, Kaur J, Kumar R. Materials today: Proceedings a review on all boron fullerene (B₄₀): A promising material for sensing and device applications. *Mater Today Proc*. 2022;**48**:1095-1102. DOI: 10.1016/j.matpr.2021.07.465
- [86] Leśnikowski ZJ. Recent developments with boron as a platform for novel drug design. *Expert Opinion on Drug Discovery*. 2016;**11**:569-578. DOI: 10.1080/17460441.2016.1174687
- [87] Ali F, Hosmane NS, Zhu Y. Boron chemistry for medical applications. *Molecules*. 2020;**25**(828):1-24. DOI: 10.3390/molecules25040828
- [88] Fink K, Uchman M. Boron cluster compounds as new chemical leads for antimicrobial therapy. *Coordination Chemistry Reviews*. 2021;**431**:213684. DOI: 10.1016/j.ccr.2020.213684
- [89] Kwiatkowska A, Sobczak M, Mikolajczyk B, Janczak S, Olejniczak AB, Sochacki M, et al. SiRNAs modified with boron cluster and their physicochemical and biological characterization. *Bioconjugation Chemistry*. 2020;**24**:1017-1026
- [90] Han Y, Wen P, Li J, Kataoka K. Targeted nanomedicine in cisplatin-based cancer therapeutics. *Journal of Controlled Release*. 2022;**345**:709-720. DOI: 10.1016/j.jconrel.2022.03.049
- [91] Tsvetkova D, Ivanova S. Application of approved cisplatin derivatives in combination therapy against different Cancer diseases. *Molecules*. 2022;**27**:2466. DOI: 10.3390/molecules27082466
- [92] Shimada M, Itamochi H, Kigawa J. Nedaplatin: A cisplatin derivative in cancer chemotherapy. *Cancer Management and Research*. 2013;**5**:67-76. DOI: 10.2147/CMAR.S35785
- [93] Musiałek MW, Rybaczek D. Hydroxyurea—The good, the bad and the ugly. *Genes (Basel)*. 2021;**12**:1096. DOI: 10.3390/genes12071096
- [94] Dawson W, Degomme A, Stella M, Nakajima T, Ratcliff LE, Genovese L. Density functional theory calculations of large systems: Interplay between fragments, observables, and computational complexity. *Wiley Interdisciplinary Reviews: Computational Molecular Science*. 2022;**12**:1574. DOI: 10.1002/wcms.1574

- [95] Maitra NT. Double and charge-transfer excitations in time-dependent density functional theory. *Annual Review of Physical Chemistry*. 2022;**73**:117-140. DOI: 10.1146/annurev-physchem-082720-124933
- [96] Sim E, Song S, Vuckovic S, Burke K. Improving results by improving densities: Density-corrected density functional theory. *Journal of the American Chemical Society*. 2022;**144**:6625-6639. DOI: 10.1021/jacs.1c11506
- [97] Urrego-Ortiz R, Builes S, Calle-Vallejo F. Impact of intrinsic density functional theory errors on the predictive power of nitrogen cycle electrocatalysis models. *ACS Catalysis*. 2022;**12**:4784-4791. DOI: 10.1021/acscatal.1c05333
- [98] Nagy Á. Fisher information and density functional theory. *International Journal of Quantum Chemistry*. 2022;**122**:e26679. DOI: 10.1002/qua.26679
- [99] Jang T, Paik D, Shin SJ, Kim H. Density functional theory in classical explicit solvents: Mean-field QM/MM method for simulating solid-liquid interfaces. *Bulletin of the Korean Chemical Society*. 2022;**43**:476-483. DOI: 10.1002/bkcs.12485
- [100] Maihom T, Sittiwong J, Probst M, Limtrakul J. Understanding the interactions between lithium polysulfides and anchoring materials in advanced lithium-sulfur batteries using density functional theory. *Physical Chemistry Chemical Physics*. 2022;**24**:8604-8623. DOI: 10.1039/d1cp05715d
- [101] Yang Y, Wang J, Shu Y, Ji Y, Dong H, Li Y. Significance of density functional theory (DFT) calculations for electrocatalysis of N₂ and CO₂ reduction reactions. *Physical Chemistry Chemical Physics*. 2022;**24**:8591-8603. DOI: 10.1039/d1cp05442b
- [102] Pernal K, Hapka M. Range-separated multiconfigurational density functional theory methods. *Wiley Interdisciplinary Reviews: Computational Molecular Science*. 2022;**12**:e1566. DOI: 10.1002/wcms.1566
- [103] Tölle J, Neugebauer J. The seamless connection of local and collective excited states in subsystem time-dependent density functional theory. *Journal of Physical Chemistry Letters*. 2022;**13**:1003-1018. DOI: 10.1021/acs.jpcclett.1c04023
- [104] Sook N, Kee Y. Assessment of CCSD (T), MP2, and DFT methods for the calculations of structures and interaction energies of the peptide backbone with water molecules. *Chemical Physics Letters*. 2017;**687**:23-30. DOI: 10.1016/j.cplett.2017.08.063
- [105] Si NT, Nhung NTA, Bui TQ, Nguyen MT, Nhat PV. Gold nanoclusters as prospective carriers and detectors of pramipexole. *RSC Advances*. 2021;**11**:16619-16632. DOI: 10.1039/D1RA02172A
- [106] Hazrati MK, Javanshir Z, Bagheri Z. B₂₄N₂₄ fullerene as a carrier for 5-fluorouracil anti-cancer drug delivery: DFT studies. *Journal of Molecular Graphics & Modelling*. 2017;**77**:17-24. DOI: 10.1016/j.jmkgm.2017.08.003
- [107] Tao Y, Chan HF, Shi B, Li M, Leong KW. Light: A magical tool for controlled. *Drug Delivery*. 2021;**30**(1-52). DOI: 10.1002/adfm.202005029
- [108] Tang Y, Wang G. NIR light-responsive nanocarriers for controlled release. *Journal of Photochemistry and Photobiology, C: Photochemistry*

- Reviews. 2021;**47**:100420. DOI: 10.1016/j.jphotochemrev.2021.100420
- [109] Kaur J, Kumar R. Borospherene - based biomarker for DNA sequencing : A DFT study. *Journal of Computational Electronics*. 2021;**20**:1916-1929. DOI: 10.1007/s10825-021-01731-6
- [110] Kaur J, Kumar R, Vohra R, Sawhney RS. Density functional theory investigations on the interaction of uracil with borospherene. *Bulletin of Materials Science*. 2022;**45**:22. DOI: 10.1007/s12034-021-02595-z
- [111] Rastgou A, Soleymanabadi H, Bodaghi A. DNA sequencing by borophene nanosheet via an electronic response: A theoretical study. *Microelectronic Engineering*. 2017;**169**:9-15. DOI: 10.1016/j.mee.2016.11.012
- [112] Yong Y, Su X, Kuang Y, Li X, Lu Z. B₄₀ and M@B₄₀ (M=Li and Ba) fullerenes as potential molecular sensors for acetone detection: A first-principles study. *Journal of Molecular Liquids*. 2018;**264**: 1-8. DOI: 10.1016/j.molliq.2018.05.046
- [113] Xiao C, Ma K, Cai G, Zhang X, Vessally E. Borophene as an electronic sensor for metronidazole drug: A computational study. *Journal of Molecular Graphics & Modelling*. 2020;**96**:107539. DOI: 10.1016/j.jmgm.2020.107539
- [114] Noroozi Z, Rahimi R, Solimannejad M. A computational study for the B₃₀ bowl-like nanostructure as a possible candidate for drug delivery system for amantadine. *Computational & Theoretical Chemistry*. 2018;**1129**:9-15. DOI: 10.1016/j.comptc.2018.02.016
- [115] Shakerzadeh E. Quantum chemical assessment of the adsorption behavior of fluorouracil as an anticancer drug on the B₃₆ nanosheet. *Journal of Molecular Liquids*. 2017;**240**:682-693. DOI: 10.1016/j.molliq.2017.05.128
- [116] Kamalinahad S, Soltanabadi A, Gamallo P. B₃₆ bowl-like structure as nanocarrier for sulfonamides: A theoretical study. *Monatshefte für Chemie*. 2020;**151**:1785-1796. DOI: 10.1007/s00706-020-02705-3
- [117] Zheng Y, Shan K, Zhang Y, Gu W. Amino acid-functionalized borospherenes as drug delivery systems. *Biophysical Chemistry*. 2020;**260**:106407. DOI: 10.1016/j.bpc.2020.106407
- [118] Yunyu Z, Jameh-Bozorghi S. Endohedral metalloborospherenes as promising drug delivery systems. *Journal of Coordination Chemistry*. 2020;**73**:1425-1435. DOI: /10.1080/00958972.2020.1788000
- [119] Deng S, Jiang Q, Wang Y, Lu X, Zhu Y, Zhang Y, et al. C₄B₃₂ nanocluster as a drug delivery system for nitrosourea anticancer drug: A first-principles perception. *Molecular Physics*. 2021;**119**:3. DOI: 10.1080/00268976.2020.1808906
- [120] Luo Q, Gu W. Novel borospherenes as cisplatin anticancer drug delivery systems. *Molecular Physics*. 2020;**118**:23. DOI: 10.1080/00268976.2020.1774088
- [121] Zhang L, Qi ZD, Ye YL, Li XH, Chen JH, Sun WM. DFT study on the adsorption of 5-fluorouracil on B₄₀, B₃₉M, and M@B₄₀ (M = Mg, Al, Si, Mn, Cu, Zn). *RSC Advances*. 2021;**11**: 39508-39517. DOI: 10.1039/D1RA08308B
- [122] Zhang L, Ye YL, Li XH, Chen JH, Sun WM. On the potential of all-boron fullerene B₄₀ as a carrier for anti-cancer drug nitrosourea. *Journal of Molecular Liquids*. 2021;**342**:117533. DOI: 10.1016/j.molliq.2021.117533

[123] Shakerzadeh E. Efficient carriers for anticancer 5-fluorouracil drug based on the bare and M-encapsulated (M=Na and Ca) B₄₀ fullerenes. In silico investigation. *J Mol Liq.* 2021;**343**:116970. DOI: 10.1016/j.molliq.2021.116970

[124] Shakerzadeh E. Endohedral M@B₄₀ (M= Na and Ca) metalloborospherenes as innovative potential carriers for chemotherapy melphalan drug: A theoretical study. *Applied Organometallic Chemistry.* 2021;**35**:e 6411. DOI: 10.1002/aoc.6411

[125] Shakerzadeh E. Li@B₄₀ and Na@B₄₀ fullerenes serving as efficient carriers for anticancer nedaplatin drug: A quantum chemical study. *Computational & Theoretical Chemistry.* 2021;**1202**:113339. DOI: 10.1016/j.comptc.2021.113339